



# The “green” use of fluorocarbons in Cherenkov detectors and silicon tracker cooling systems: challenges and opportunities in an unfolding era of alternatives

G. D. Hallewell<sup>a</sup>

Aix Marseille Université, CNRS/IN2P3, CPPM, Marseille, France

Received: 30 April 2023 / Accepted: 16 November 2023  
© The Author(s) 2023

**Abstract** Saturated fluorocarbons (SFCs) of form  $C_nF_{(2n+2)}$  are chosen for their optical properties as Cherenkov radiators, with  $C_4F_{10}$  and  $CF_4$  currently used at CERN in the COMPASS and LHCb ring imaging Cherenkov detectors. Their non-conductivity, non-flammability and radiation-resistance also make SFCs ideal coolants:  $C_6F_{14}$  liquid cooling is used in all LHC experiments, while  $C_3F_8$  is used for the evaporative cooling of TOTEM and the ATLAS silicon tracker. These fluids, however, have high global warming potentials ( $5000\text{--}10000 \times GWP_{CO_2}$ ), and represented around 36% of CERN’s  $CO_2$ -equivalent emissions in 2018. There is thus an impetus to reduce their use, losses in purification and wastage through leaks, through improved monitoring and closed circulation system design. Newer spur-oxygenated fluoro-ketones, for example from the 3 M NOVEC<sup>®</sup> range, with  $C_nF_{2n}O$  structures, can offer similar performance to SFCs with but with very low, or zero GWP. Although these fluids do not yet exist in large quantities over the full  $C_nF_2$  “matrix” the radiation tolerance and thermal performance of NOVEC 649 ( $C_6F_{12}O$ ) was sufficiently promising for it to be chosen as a  $C_6F_{14}$  replacement for cooling silicon photomultipliers. Additionally, subject to optical testing, NOVEC 5110 ( $C_5F_{10}O$ ) could (if blended with nitrogen) replace both  $C_4F_{10}$  and  $CF_4$  in Cherenkov detectors. Lighter molecules (for example  $C_2F_4O$ , with similar thermodynamics to  $C_2F_6$ )—if and when available in industrial quantities—might allow lower temperature operation than evaporative  $CO_2$  in future silicon trackers operated at very high luminosity. Ultrasonic gas mixture analysis is very sensitive to concentration changes of a heavy vapour in a light carrier, and is used—in the only such fluorocarbon coolant leak monitoring system operating at LHC—for real-time monitoring of  $C_3F_8$  coolant leaks from the ATLAS pixel and SCT silicon trackers into their nitrogen-flushed environmental volumes. A typical  $C_3F_8$  sensitivity of better than  $10^{-5}$  is achieved. Advanced new ultrasonic algorithms allow measurement of the concentrations of a pair of gases of particular interest on top of a varying known baseline of other gases. The technique is thus of considerable value in leak monitoring and could be used to blend fluoro-ketones with nitrogen or argon to reduce the GWP “load” of large volume atmospheric pressure gas Cherenkov radiators without the recourse to higher-pressure noble gas approaches. This paper outlines an approach to GWP reduction with fluoro-ketone fluids and the blending of heritage SFCs or fluoro-ketones with lighter gases using ultrasonic monitoring and control. Possible avenues for the use of fluoro-ketones in liquid phase and evaporative cooling of silicon trackers are discussed.

## Abbreviations

ALICE	(“A Large Ion Collider Experiment”): a detector dedicated to heavy-ion physics at the CERN Large Hadron Collider (LHC)
ATLAS	(“A toroidal LHC apparatus”): the largest general-purpose particle detector at the CERN LHC, implementing solenoidal and toroidal magnetic fields
ATLAS SCT	(“Semi-conductor tracker”): the silicon micro-strip component of the ATLAS inner tracker
ATLAS IBL	(“Insertable B layer”): a cylindrical silicon pixel detector layer upgrade to the ATLAS silicon tracker: inserted within 3 cm of the colliding LHC beams
BTeV	(“B meson TeV”) experiment to study CP violation, mixing and rare decays of bottom and charm quark states at the FNAL Tevatron, scheduled start 2006, project cancelled early 2005
CERN	The European particle physics laboratory, Geneva, Switzerland
Cherenkov Radiation	Electromagnetic radiation (peaked in the ultraviolet) emitted by charged particles traversing a transparent medium at a velocity exceeding the velocity of light in that medium: used as a tool for particle identification
Cherenkov radiator	A transparent medium (solid, liquid or gas) with refractive index chosen to optimise particle identification over a specific energy range

<sup>a</sup> e-mail: [gregh@cppm.in2p3.fr](mailto:gregh@cppm.in2p3.fr) (corresponding author)

CMS	("Compact muon solenoid"): A large general-purpose detector at the CERN LHC implementing a large instrumented solenoidal magnetic field
CMS TIB, TID, TOB & TEC	Elements of the CMS silicon microstrip tracking detector: respectively "tracker inner barrel", "tracker inner disks, "tracker outer barrel"& "tracker end caps"
COMPASS	("Common muon proton apparatus for structure and spectroscopy") an experiment using CERN SPS high-intensity muon and hadron beams for the investigation of the nucleon spin structure and hadrons
CRID	Cherenkov ring imaging detector
DELPHI	(Detector with lepton, photon and hadron identification) a large detector at the CERN large electron-positron collider (lep) with specific focus on particle identification (operation 1989–2000)
DESY	(Deutsches elektronen-synchrotron) German national particle physics laboratories in Hamburg and Zeuthen
Fluorinert®	A product range nomenclature of the 3 M Corporation for saturated fluorocarbons of chemical form $C_nF_{(2n+2)}$ for use in a variety of cooling, semiconductor manufacture and medical applications
Fluoro-ketones	Fluorinated molecules with a $-C(=O)-$ carbonyl group containing a carbon-to-oxygen double bond ( $C=O$ )
FNAL	Fermi national accelerator laboratory, Batavia, Illinois, USA
GeV	A unit of energy ( $10^9$ electronvolts)
GSI	The GSI Helmholtzzentrum für Schwerionenforschung, accelerator centre in Darmstadt Germany
HADES	High-acceptance di-electron spectrometer); operating at the GSI SIS18 heavy ion synchrotron
HERA	(Hadron–electron ring accelerator): electron/positron-proton collider at DESY Hamburg (operation 1992–2007)
HERA-B	A detector for the study of CP violation in the decays of heavy B mesons at the HERA collider at the German national particle physics laboratory DESY, Hamburg (operation 1999–2003)
Gray (Gy)	S.I. unit of ionizing radiation dose-defined as the absorption of 1 Joule of radiation energy per kg of matter
GWP	Global warming potential
LHC	The CERN Large hadron collider (operational since 2008)
LHCb	(Large hadron collider beauty) a specialized b-physics experiment, designed primarily to measure the parameters of CP violation in the interactions of b-hadrons (heavy particles containing a bottom quark)
LHCb VELO	The LHCb "vertex locator": multiplane silicon pixel detector close to the LHC colliding beams
NA62	An experiment at the North Hall of the CERN SPS aiming to study the decay $K^+ \rightarrow \pi^+ + \nu\nu^-$
NOVEC®	A product range nomenclature of the 3 M Corporation for low GWP replacements for saturated fluorocarbons and SF <sub>6</sub> , including (amongst other fluids) fluoro-ketones of chemical form $C_nF_{2n}O$ for use in cooling, semiconductor manufacture and inert gas fire-fighting applications
OMEGA	A large aperture superconducting dipole spectrometer that operated at the West Hall of the CERN SPS (operation 1972–1996)
RICH	Ring imaging cherenkov detector
Roman Pot	A vessel with a very thin metallic window separating the accelerator vacuum from a detector operating close to the circulating beams
SiPM	Silicon photomultiplier - a semiconductor-based (rather than vacuum based) single photon detector
SLAC	Stanford linear accelerator center (Stanford University) aka SLAC national accelerator laboratory
SLC	Stanford linear collider: the World's first and only operational linear collider, accelerating and colliding electron and positron beams at a centre-of-mass energy equivalent to the Z boson mass (operation 1988–1998)
SLD	The SLAC large detector: the main detector at SLC-designed primarily to detect Z bosons (operation 1992–1998)
SPS	The CERN super proton synchrotron (operational since 1976)
SFC	Saturated fluoro-carbons: fluorinated molecules having single Carbon-Fluorine bonds and chemical structure $C_nF_{(2n+2)}$
Tevatron	Proton-antiproton collider at the Fermi National Accelerator Laboratory (operation 1983–2011)
Thermal Figure of Merit (TFM)	Expressed in terms of the temperature difference between a silicon detector module and the cooling fluid for a given power density (units of $^{\circ}C\ cm^2\ W^{-1}$ ) as $(T(\text{Si module}) - T(\text{Coolant})) / (\text{Si module power}/cm^2)$ . The lower the numeric value the better the thermal performance. (§5.1)
TOTEM	(Total elastic and diffractive cross section measurement): an experiment at the CERN LHC
VHMPID	(Very high momentum particle identification detector): a proposed upgrade detector for the ALICE experiment at the CERN LHC

## 1 Introduction

Saturated fluorocarbons (SFCs) have been historically chosen as RICH detector radiators for their optical properties. The CERN OMEGA RICH used a blended  $C_2F_6/N_2$  radiator, while the DELPHI RICH and SLD CRID detectors combined  $C_6F_{14}$  as a liquid radiator with  $C_4F_{10}$  and  $C_5F_{12}$  or  $87\%C_5F_{12}/13\%N_2$  as gaseous radiators. The ALICE HMPID presently uses  $C_6F_{14}$  as a liquid radiator. The HADES and HERA-B RICH detectors used  $C_4F_{10}$  while the COMPASS and LHCb RICH detectors currently use  $C_4F_{10}$  and  $CF_4/CO_2$ <sup>1</sup> gas radiators.

SFC fluids are non-toxic, non-conductive, non-flammable and radiation resistant: properties that have also made them ideal coolants for electronics and semiconductor tracking detectors. Although non-ozone-depleting, these fluids exhibit very high Global Warming Potentials (GWPs); typically in the range 5000–9000, and represented around 36% of CERN's  $CO_2$  and  $CO_2$ -equivalent direct emissions in 2018. Other fluorinated compounds including HFCs and  $SF_6$  contributed 57% to CERN's direct emissions total [1–4]. There is thus an impetus to reduce the use of fluorinated fluids, and equally-importantly their loss in purification and wastage through leaks [5], with improved monitoring and closed-circuit circulation system design.

Fluoro-ketones with alternative  $C_nF_{2n}O$  molecular structures have also been studied as Cherenkov gas radiators; 3 M PFG-3480 [6] octofluorotetra-hydrofuran (c- $C_4F_8O$ ) for BTeV [7] and Synquest 2H07-2-08 c- $C_4F_8O$  [8] for the ALICE VHMPID [9]. While offering similar optical performance to SFCs of the same order,  $n$ , their GWPs were not lower, due to their robust closed molecular ring geometry incorporating the oxygen atom as an internal link. Indeed, the GWP of this fluid has been estimated [10] to be 8975, 12 000, and 16 000, respectively, for the 20-, 100-, and 500-year time horizons. Such closed ring molecular geometries are clearly to be avoided.

The newer 3 M NOVEC<sup>®</sup> range of fluoroketone fluids [11] currently includes two with non-cyclic (spurred)  $C_nF_{2n}O$  molecular forms. These fluids; NOVEC 649/1230 (Perfluoro-2-methyl-3-pentanone, CAS 756-13-8: molecular formula  $C_2F_5C(O)CF(CF_3)_2$ :  $C_6F_{12}O$  or “C6K” for short) [12] and NOVEC 5110 (Perfluoro-2-methyl-3-butanone, CAS No. 756-12-7:  $CF_3C(O)CF(CF_3)_2$ :  $C_5F_{10}O$  or “C5K” for short) [13] have GWPs of  $\leq 1$  and are of interest at CERN. As in the case of the SFCs, these fluids are non-flammable, non-toxic, non-conductive and non -ozone-depleting. The radiation tolerance of NOVEC 649 has been tested and looks encouraging [14] for use as a liquid coolant in high radiation zones near the LHC beams. Such attractive non-cyclic  $C_nF_{2n}O$  fluids do not however, yet exist in industrial quantities at the “light” ( $n < 4$ ) end of the  $C_nF_{2n}$  “spectrum”: their future industrialization will probably be dominated by the needs of the electronics industry. Figure 1 illustrates the molecular shapes of the saturated fluorocarbons, commonly used as gaseous Cherenkov radiators and detector coolants, along with their 20-year GWPs. Beneath these are shown the shapes of non-cyclic (spurred)  $C_nF_{2n}O$  analogues. This geometry is currently exemplified by NOVEC 5110 and NOVEC 649, which are in large-scale production. A study of the decomposition of spurred, non-cyclic  $C_6F_{12}O$  [15] has shown that scission of the linear molecule on either side of the side-branched oxygen atom by UV photons of around 300 nm in the low pressure of the upper atmosphere results in decomposition products that do not contribute to global warming.

It can be seen from Fig. 1 that as the order  $n$  of the  $C_nF_{2n}O$  molecule increases so does the number of isomers can become available. Several of these are shown in Fig. 2 for the example of  $C_4F_8O$ .

While the cyclic geometry is known to have a very high GWP, it is likely that geometries with the oxygen atom on a spur or the end of the molecule will have very low GWPs, as in the case of NOVEC5110 ( $C_5F_{12}O$ ). Non-cyclic geometries with the oxygen atom as an internal link and a double carbon bond elsewhere in the molecule could have intermediate GWP: these would need to be studied.

While the optical constraints of RICH detectors might motivate a “special case” argument for continued use of known and preferred SFCs, legislation and external market forces will limit their future availability (for example through reduced industrial demand in applications such as vapour phase reflux soldering in the computer industry), leaving “holes” in the  $C_nF_{2n}$  spectrum that might not be filled by suitable  $C_nF_{2n}O$  equivalents.

The use of flammable radiator gases such as isobutane ( $C_4H_{10}$ ; GWP = 3.3) or use of pressurised noble gases has been mooted [16, 17] but neither option is particularly attractive, respectively, due to restrictions on the use of large volumes of flammable gases in underground areas and concerns for the large *pressure\*volume* (PV) stored energy in radiator vessels of volumes of order  $100\text{ m}^3$  similar to those of LHCb RICH-1 & 2.

An alternative solution might involve the blending of low molar concentrations of heritage higher-order SFCs or fluouo-ketone vapours with transparent lighter gases. For example  $C_4F_{10}$  from stock kept at CERN for the COMPASS and LHCb RICH-1 radiators could be blended at low molar concentration with nitrogen to replicate the refractive index of  $CF_4$  in the LHCb RICH-2 radiator at a lower GWP, as discussed in §2.

While continuous optical measurement of refractive index in dynamically changing gas mixtures can be very demanding, the monitoring of sound velocity has been shown to provide simple, reliable and continuous real time mixture information. Indeed the speed of sound in the gas radiator of a Cerenkov detector is in itself a monitor of the speed of light, and with it the thresholds in GeV for particle species  $e^\pm$ ,  $\mu^\pm$ ,  $p^\pm$ ,  $K^\pm$ ,  $p^\pm$ . This ultrasonic (“sonar”) technique was first used for controlling the real-time blending of  $C_5F_{12}$  with  $N_2$  in a 87%/13% ratio for the SLD CRID at the SLAC linear collider.

<sup>1</sup> A few %  $CO_2$  is added to quench  $CF_4$  scintillation light.

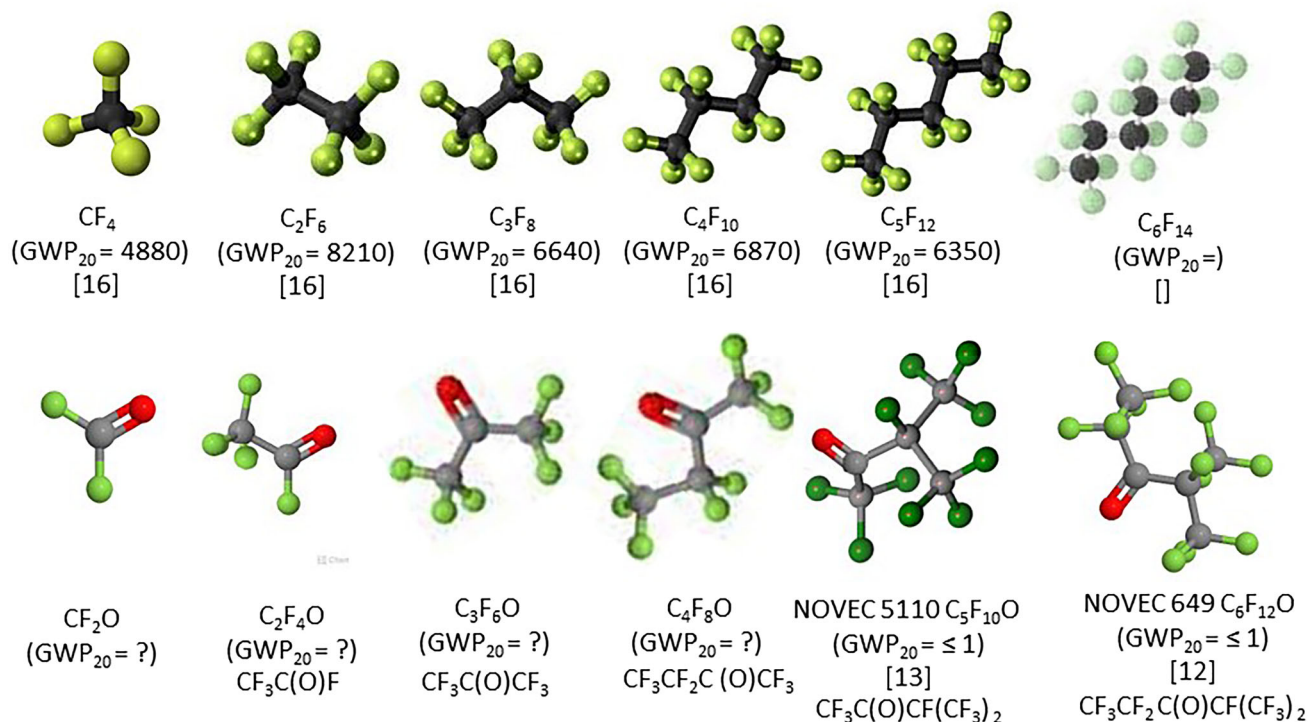


**Fig. 1** Upper: molecular shapes of SFCs, including some commonly used as gaseous Cherenkov radiators and tracking detector coolants; lower: shapes of some non-cyclic C<sub>n</sub>F<sub>2n</sub>O analogues with fluorine and oxygen atoms, respectively, shown green and in red. 20-year GWPs are noted where known

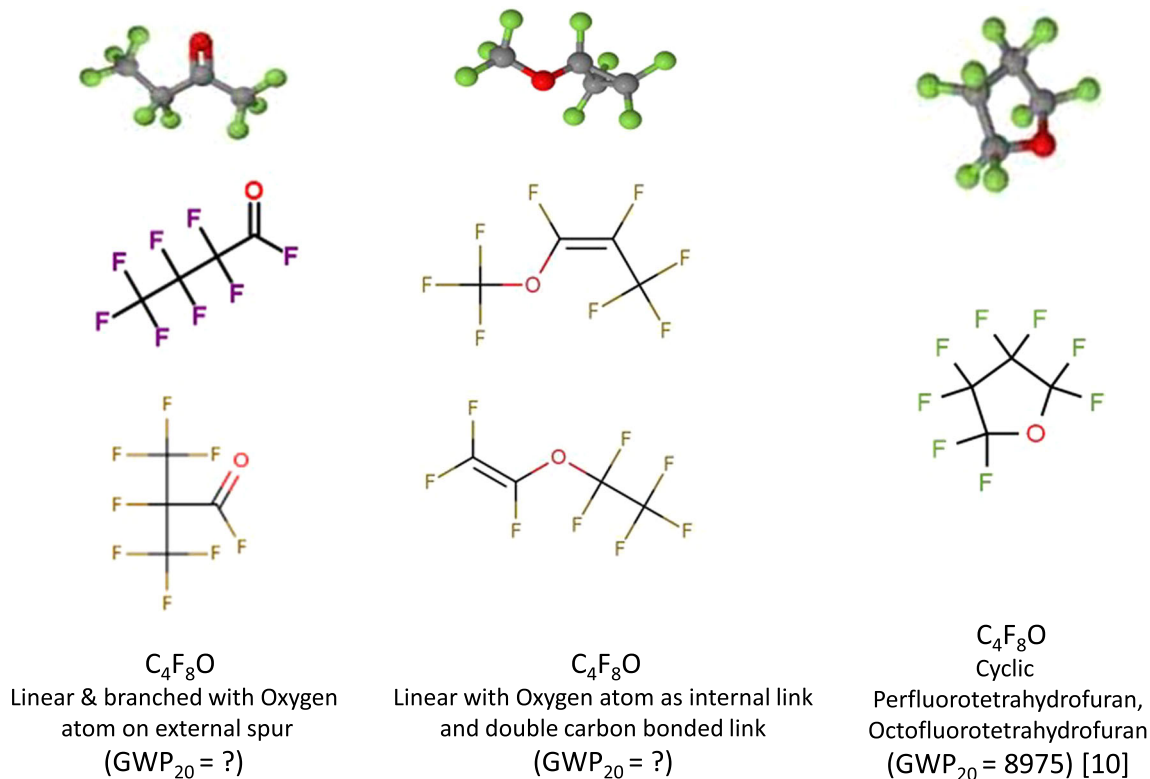


**Fig. 2** Shape examples of cyclic, non-cyclic and non-cyclic double carbon-bonded C<sub>4</sub>F<sub>8</sub>O isomers

The technique could become important again in future operation to match the dual constraints of optical properties and low radiator GWP. The methodology, illustrated with some examples, is explored in the following sections.

## 2 GWP reduction in Cherenkov gas radiators: motivation and methodology

Three large ring imaging Cherenkov detectors are currently in operation at CERN. These detectors have radiator gas volumes of the order of 100 m<sup>3</sup> and use saturated fluorocarbons: C<sub>4</sub>F<sub>10</sub> in the COMPASS RICH and LHCb RICH 1, and CF<sub>4</sub> in LHCb RICH 2. These vapours have 20-year global warming potentials of 4880 and 6870, respectively.

A Cherenkov radiator vessel of volume  $V(\text{m}^3)$  filled with a blend of gases of densities  $\rho_i$  (kg m<sup>-3</sup>), molar concentrations  $w_i$  and individual Global Warming Potentials  $\text{GWP}_i$  can be considered to have a GWP environmental “load” (and release potential)  $L$  (in tonnes CO<sub>2</sub> equivalent) given by:

$$L = \frac{V}{1000} \sum_i \omega_i \cdot \rho_i \cdot \text{GWP}_i \tag{1}$$

From the molar concentrations  $w_i$  of the components the refractivity of the radiator gas mixture,  $(n - 1)_{\text{rad}}$ , can be calculated according to:

$$(n - 1)_{\text{rad}} = \sum_i \omega_i (n - 1)_i \tag{2}$$

From eqs. (1) and (2) it can be seen how the blending of a high refractivity (heavier) SFC or NOVEC vapour with a light transparent gas (or gases) might result in optical properties equivalent to those of a lighter SFC at 100% molar concentration, but with a lower overall GWP load. In this context the replacement of a lighter SFC by a (GWP = 1) “NOVEC” fluoro-ketone alternative would be ideal, but the absence of convenient NOVEC fluids blends of legacy stock heavier SFCs could be considered. Taking the case of a binary mixture of a heavy fluoro-ketone or SFC vapour  $x$  of refractivity  $(n - 1)_x$  a light transparent partner  $y$  of refractivity  $(n - 1)_y$ , the molar concentration,  $w_x$ , necessary to replicate the refractivity of a light SFC  $z$  with refractivity  $(n - 1)_z$  can be expressed as:

$$w_x = \frac{((n - 1)_z - (n - 1)_y)}{((n - 1)_x - (n - 1)_y)} \tag{3}$$

Some examples of GWP environmental load are explored in table 1, assuming a Cherenkov radiator volume of 100 m<sup>3</sup> and an operating pressure of 10<sup>5</sup> hPa (1 bar<sub>abs</sub>). In each case comparisons are made with the “target” SFC—taken as either CF<sub>4</sub> and C<sub>4</sub>F<sub>10</sub> (vapours of current use in the COMPASS and LHCb RICH detectors)—as single component radiators. The molar concentration  $w_x$  in nitrogen  $((n - 1)_y = 310 \times 10^{-6})$  of the alternative SFC or NOVEC vapour is chosen to give a similar refractivity to pure CF<sub>4</sub>  $((n - 1)_z = 488 \times 10^{-6})$  or C<sub>4</sub>F<sub>10</sub>  $((n - 1)_z = 1450 \times 10^{-6})$ . Table 1 also shows the positions of “fantasy” fluids (*in italic text*) in the  $C_n F_{2n}$  “matrix” that do not currently exist in large quantities. In the case of non-cyclic C<sub>4</sub>F<sub>8</sub>O the average refractive index is assumed from measurements made in the studies for BTeV [7] and the ALICE VHMPID [9] for cyclic C<sub>4</sub>F<sub>8</sub>O.

The uncertainties that exist in the refractivities of non-cyclic C<sub>4</sub>F<sub>8</sub>O and NOVEC 5110 render Table 1 only an indicator of what may be achievable. Perhaps this will also serve as a stimulus for future optical measurements in these fluids.

From Table 1 it can be seen that reductions in GWP load can be made by the replacing pure CF<sub>4</sub> and pure C<sub>4</sub>F<sub>10</sub> radiators with heavier order SFCs or  $C_n F_{2n} O$  vapours blended with N<sub>2</sub>. In CF<sub>4</sub> replacement the best reduction in GWP load that can be expected with higher order SFCs is 44.9% using C<sub>5</sub>F<sub>12</sub> at 13% molar concentration. The corresponding reduction through the use of C<sub>4</sub>F<sub>10</sub> at 16.3% molar concentration is 35.6%. In the case of replacement with C<sub>2</sub>F<sub>6</sub> and C<sub>3</sub>F<sub>8</sub> the gains are less, partly due to the higher molar concentrations required, and (particularly in the case of C<sub>2</sub>F<sub>6</sub>) the higher GWP. Of course, the reduction of the 100 m<sup>3</sup> radiator GWP load through the replacement of CF<sub>4</sub> with 13.9% NOVEC5110 would be total, as it would be also for a hypothetical non-cyclic C<sub>4</sub>F<sub>8</sub>O vapour blended at 18.4%.

In the case of C<sub>4</sub>F<sub>10</sub> replacement there is naturally less room to manoeuvre, with the only practical high order alternatives being C<sub>5</sub>F<sub>12</sub> or NOVEC 5110. A reduction in GWP load of 14.5% can be expected with C<sub>5</sub>F<sub>12</sub> at 79% molar concentration. The reduction of the 100 m<sup>3</sup> radiator GWP load through substitution of C<sub>4</sub>F<sub>10</sub> with NOVEC 5110 at 85% molar concentration is total, of course. Since the boiling points of C<sub>5</sub>F<sub>12</sub> and NOVEC 5110 at atmospheric pressure are, respectively, 30 and 27 °C it may be necessary to warm the outer surface of the Cherenkov radiator vessel above this temperature when high concentrations of these vapours are used. Fluids of higher order such as C<sub>6</sub>F<sub>14</sub> and C<sub>6</sub>F<sub>12</sub>O (NOVEC 649/1230) with correspondingly higher boiling temperatures (respectively 56 and 49 °C) are not therefore considered for use as gas radiator components due to the correspondingly higher radiator vessel temperatures that would be required.

GWP reduction through blending has been illustrated in Table 1. The following section discusses ultrasonic methodology for the continuous monitoring of Cherenkov radiator gas blends.

## 3 The blend monitoring approach

In the domain of Cherenkov detectors radiator refractive index,  $n$ , is of primary physics importance and can be monitored directly by the extraction of gas to optical interferometers, including Fabry–Perot devices. The operation of such devices is however complex

**Table 1** GWP loads of various SFCs and NOVEC 5110 blended with N<sub>2</sub> ((*n*-1) = 310 × 10<sup>-6</sup>) to match refractivity of CF<sub>4</sub> and C<sub>4</sub>F<sub>10</sub>

Base fluid	Base fluid density (1 bar, 25 °C) kgm <sup>-3</sup>	Base fluid GWP (20-yr)	Component ( <i>n</i> - 1) (*10 <sup>6</sup> ) (@ nm)	% Blend with N <sub>2</sub> to match ( <i>n</i> - 1) CF <sub>4</sub>	GWP load (tCO <sub>2</sub> )	% Blend with N <sub>2</sub> to match ( <i>n</i> - 1) C <sub>4</sub> F <sub>10</sub>	GWP load (tCO <sub>2</sub> )
<b>CF<sub>4</sub></b>	<b>3.56 [18]</b>	<b>4880 [16]</b>	<b>488 (180–310 nm) [19]</b>	<b>100</b>	<b>1737</b>	<b>Not applicable</b>	<b>n/a</b>
CF <sub>2</sub> O	–	–	–	–	–	<i>n/a</i>	<i>n/a</i>
C <sub>2</sub> F <sub>6</sub>	5.63 [18]	8210 [16]	793 (180–310 nm) [19]	38.1	1762	Not applicable	<i>n/a</i>
<i>Lin</i> -C <sub>2</sub> F <sub>4</sub> O	–	–	–	–	–	<i>n/a</i>	<i>n/a</i>
C <sub>3</sub> F <sub>8</sub>	7.75 [18]	6640 [16]	1180 (250 nm) [16]	21.4	1099	Not applicable	<i>n/a</i>
<i>Lin</i> -C <sub>3</sub> F <sub>6</sub> O	–	–	–	–	–	<i>n/a</i>	<i>n/a</i>
<b>C<sub>4</sub>F<sub>10</sub></b>	<b>9.97 [18]</b>	<b>6870 [16]</b>	<b>1450 (250 nm) [16]</b>	<b>16.3</b>	<b>1119</b>	<b>100</b>	<b>6849</b>
<i>Lin</i> -C <sub>4</sub> F <sub>8</sub> O ( <i>Non</i> -cyclic C <sub>4</sub> F <sub>8</sub> O)*	9.5 ( <i>est.</i> )	<i>Probably</i> < 1 (NOVEC 5110 <i>Analogy</i> )	1380 @ 400 nm ( <i>based on 3 M</i> PFG-3480 <i>c</i> -C <sub>4</sub> F <sub>8</sub> O [7]: <i>linear C<sub>4</sub>F<sub>8</sub>O not</i> <i>yet measured but</i> <i>assumed similar</i> )	18.4	0.18	112.7* (> 100% would <i>imply necessity of</i> <i>operating C<sub>4</sub>F<sub>8</sub>O at</i> <i>slight overpressure</i> )	1.07
C <sub>5</sub> F <sub>12</sub>	11.63 [18] (BP 30 °C at 1 bar)	6350 [16]	1750 (180–310 nm) [19] (40 °C, undiluted)	13.0	957	79.3	5857
NOVEC 5110 C <sub>5</sub> F <sub>10</sub> O	10.7 [13] (BP 27 °C at 1 bar)	< 1 [13]	Not yet measured: probably around 1650 by analogy with C <sub>4</sub> F <sub>10</sub> and C <sub>4</sub> F <sub>8</sub> O ratio	13.9	0.149	85.2	0.91

Lines in the table corresponding to presently unavailable-in-bulk C<sub>n</sub>F<sub>m</sub>O fluids are shown in *italics*. Lines corresponding to the molecules CF<sub>4</sub> and C<sub>4</sub>F<sub>10</sub>, whose optical parameters are targeted for matching, are shown in **bold** text. GWP loads and refractivities are calculated using eqs. (1–3)

\*Made in research quantities by Synquest Inc. as isomers heptafluorobutyl fluoride PN: 2116-2-07 CAS: 335-42-2 Octafluoro-2-butanone PN: 2117-2-10 CAS: 337-20-2 & heptafluoroisobutyl fluoride PN: 2116-2-0A CAS: 677-84-9

and they cannot be classified as continuously-sensitive instruments providing unattended 24/7 monitoring. Indirect measurement of gas refractive index from prior knowledge of the molar concentrations,  $w_i$ , of the component gases using Eq. (2) is an alternative.

While component concentration in gas blends may be monitored by various optical, chemical and thermal methods, a particularly robust method uses ultrasonic measurements of sound velocity in the gas blend. Ultrasonic monitoring of refractive index for real-time blending of gas mixtures was first used in the 1990s for  $C_5F_{12}/N_2$  blending in the SLD CRID at the SLAC linear collider [20–22]. Such a technique could be used in the future, blending SFCs or FCOs with nitrogen or argon to reduce the GWP “load” of large volume atmospheric pressure gas Cherenkov radiators. Advanced new ultrasonic algorithms [23] allow analysis of mixtures containing more than two gases; specifically the concentrations of a pair of gases of particular interest (for example a fluorocarbon vapour in nitrogen) on top of a varying known baseline of other gases. These techniques are discussed in §3.1–3.4.

### 3.1 Measurement of sound velocity

Sound velocity in a Cherenkov radiator is measured from transit time over known distances in gas at known temperature and pressure. Ultrasonic transducers may be placed *in-situ* within the radiator vessel [20–22], in aspirating sample stations or in the gas circulation piping system where they can provide a simultaneous flow measurement in a single instrument [23]. Starting with the installation in the SLD CRID [20–22], most implementations [24–27] have used the 50 kHz capacitive ultrasonic transducer [28] first developed for Polaroid autofocus cameras. The relatively high bias voltages (up to 350 V) that can be applied to these transducers results in reduced jitter compared with many piezoelectric transducers. Their disadvantage lies in an operating frequency close to the maximum of the  $CO_2$  ultrasound absorption peak running from 10–100 kHz (FWHM), which makes them unsuitable for use in high  $CO_2$  concentrations where piezoelectric transducers with frequencies of 200 kHz or more are better adapted.

Despite its success in the SLD CRID [20–22], continuous on-line ultrasonic *in-situ* measurement of Cherenkov gas radiator refractive index has been less fully exploited in current RICH detectors. This is surprising, since it is ideally suited to monitoring hydrostatic variations in refractive index, in monitoring and maintaining a blend of gases as well as its evolution during the replacement of a passivation gas (e.g.  $N_2$ ) with the radiator gas. It is a promising technique in the blending SFC or NOVEC vapours with light gases for GWP load reduction.

### 3.2 Sound velocity calculation for a database

The technique exploits the dependence of sound velocity on the molar concentrations of components of differing molecular weight (m.w.) at known temperature and pressure. Look-up tables of *molar concentration versus sound velocity* are set up using the general formalism expressing the sound velocity,  $v_s$ , in terms of the thermodynamic properties of the component gases:

$$v_s = \sqrt{\frac{\gamma_m \cdot R \cdot T}{M_m}} \tag{4}$$

where  $\gamma_m$  is the adiabatic index for the mixture,  $R$  is the molar gas constant ( $8.3145 \text{ J}\cdot\text{mol}^{-1}\cdot\text{K}^{-1}$ ),  $T$  is the absolute temperature (K) and  $M_m$  is the combined molar mass of the mixture.

$M_m$  and  $\gamma_m$  are given, respectively, by:

$$M_m = \sum_i \omega_i M_i \quad \text{and} \quad \gamma_m = \frac{\sum_i \omega_i C_{P_i}}{\sum_i \omega_i C_{V_i}} \tag{5}$$

where  $\omega_i$  is the molar fraction of component  $i$  in the mixture while  $C_{P_i}$  and  $C_{V_i}$  are its molar specific heats at constant pressure and volume, respectively.

Figure 3 illustrates the temperature and pressure variation of  $C_p$  and  $C_v$  in pure  $C_4F_{10}$  and pure  $N_2$ , calculated with the REFPROP (Reference Fluid thermodynamic & Transport Properties) package using NIST standard reference database 23, version 9 (2010) [18]. This gas combination is relevant as the base radiator and passivation gas in the LHCb RICH-1 [25, 26] and the COMPASS RICH [5, 27] and also as a GWP load-reducing match to the refractivity of  $CF_4$  in LHCb RICH-2 (§1, Table 1). The temperatures shown cover a wide operating range while the (950–1050 mbar<sub>abs</sub>) pressure range assumes a radiator vessel referenced to atmosphere.

Data of the type illustrated in Fig. 3 are combined via Eqs. (4) & (5) to generate a look-up table of polynomial fit parameters to curves of  $C_4F_{10}/N_2$  molar concentration  $w_x$  versus sound velocity at points on a grid covering a range of temperature and pressure. Figure 4 illustrates (also in the context of Cherenkov thresholds: §3.3) one such curve (*referenced to right vertical axis*) calculated at 25 °C and 1000 hPa.

An accurate fit to this curve over the full  $C_4F_{10}/N_2$  concentration range requires a quartic polynomial of the form:

$$w_{C_4F_{10}}(\%) = \alpha \cdot V_s^4 + \beta \cdot V_s^3 + \gamma \cdot V_s^2 + \delta \cdot V_s + \varepsilon \tag{6}$$

The fit parameters to such curves can be thought of as being stored in ‘cans’ suspended at the  $\{T, P\}$  intersection points on a two-dimensional mesh (Fig. 5). In practice, of course, sound velocity is measured at temperatures and pressures falling between the  $\{T, P\}$  intersections. Fit parameters must therefore be interpolated from “*can values*” to generate new parameters corresponding to the measured temperature  $T_{\text{meas}}$  and pressure  $P_{\text{meas}}$  from which  $w_{C_4F_{10}}$  can then be calculated using Eq. (6).

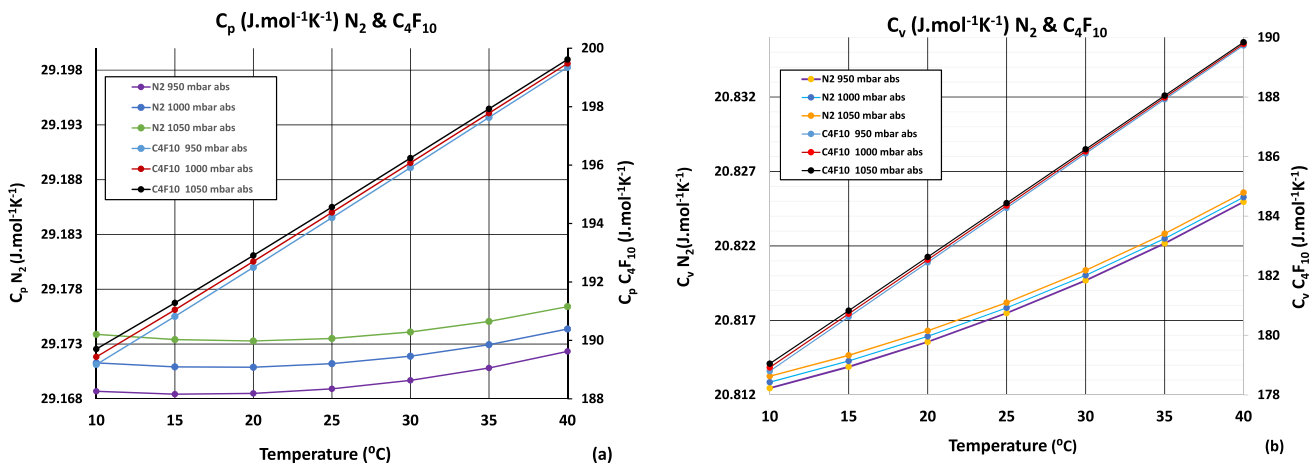


**Fig. 3** Left: Molar specific heat at constant pressure versus temperature for  $\text{N}_2$  (left axis) and  $\text{C}_4\text{F}_{10}$  (right axis) at a range of temperatures and pressures: Right: Molar specific heats at constant volume over the same range of temperatures and pressures

**Fig. 4** Left: Cherenkov thresholds for particle species versus measured sound velocity in a radiator gas combining  $\text{C}_4\text{F}_{10}$  with  $\text{N}_2$ . Right:  $\text{C}_4\text{F}_{10}$  concentration. The  $\text{C}_4\text{F}_{10}$  concentration to match the  $p^\pm$ ,  $K^\pm$  &  $\pi^\pm$  thresholds of the LHCb RICH-2  $\text{CF}_4$  radiator (with much lower GWP load: Table 1) is also shown on the right axis

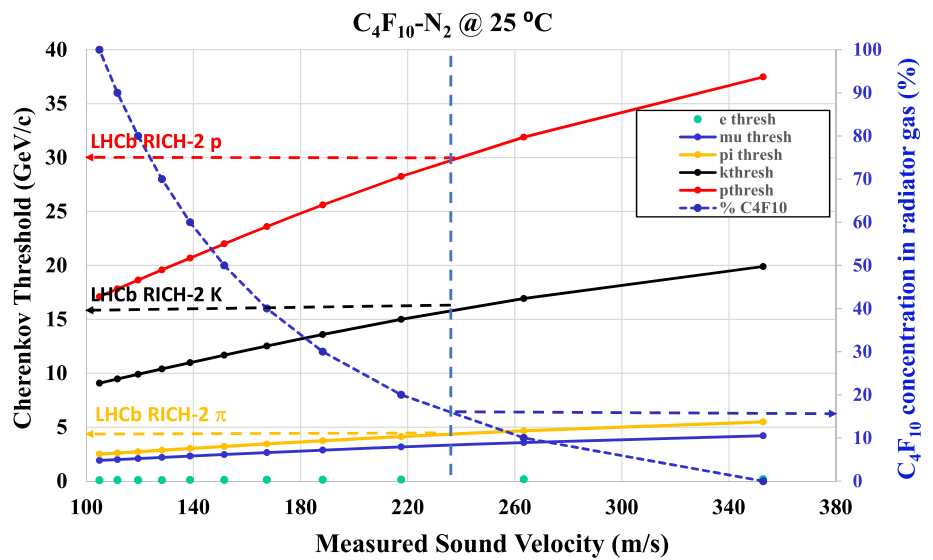
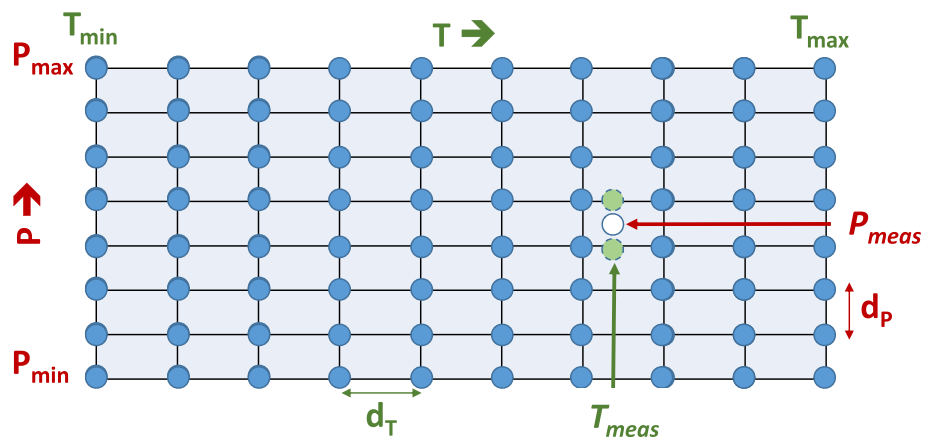


**Fig. 5** Illustration of the two-step interpolation of sound velocity versus molar concentration fit parameters held in ‘cans’ (·) at the nearest stored grid intersections to determine those corresponding to the measured  $\{T, P\}$  process conditions. ‘Temporary cans’ are shown in green

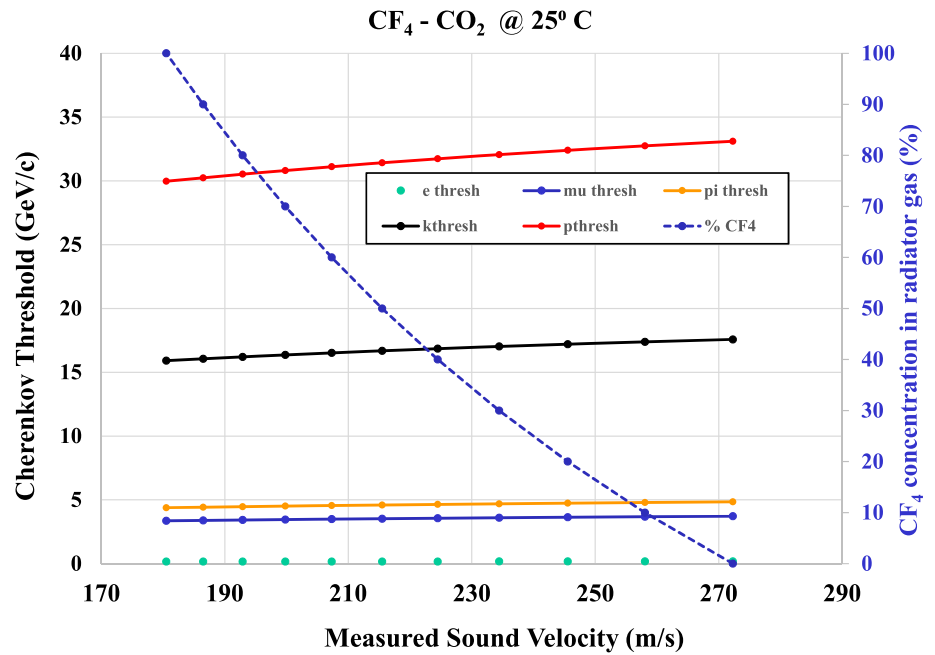


Parameters can first be interpolated (linearly or otherwise depending on the grid spacing) to intermediate values corresponding to  $T_{\text{meas}}$  at grid pressures in new, temporary ‘cans’ immediately above and below  $P_{\text{meas}}$ :

$$\{\alpha, \beta, \gamma, \delta, \varepsilon @ (T_{\text{meas}}, P > P_{\text{meas}})\}, \{\alpha, \beta, \gamma, \delta, \varepsilon @ ((T_{\text{meas}}, P < P_{\text{meas}}))\}.$$



**Fig. 6** Cherenkov thresholds (left axis) for particle species versus sound velocity in a radiator gas combining CF<sub>4</sub> with CO<sub>2</sub> at 25 °C: right axis, CF<sub>4</sub> concentration



A second interpolation between these intermediate fit parameters along the orthogonal (pressure) direction calculates final parameters corresponding to both  $T_{meas}$  &  $P_{meas}$ :  $\{\alpha, \beta, \gamma, \delta, \epsilon @ (T_{meas}, P_{meas})\}$  from which the relative concentrations of the two components can be calculated.

The precision of mixture determination,  $\delta(w_i)$ , can be expressed as;

$$d(w_i) = m \times \delta V_s \tag{7}$$

where  $m$  is the local slope of the *concentration versus sound velocity* dependence.

The sound velocity precision,  $\delta V_s$ , of modern versions of the instrument [23] developed for monitoring C<sub>3</sub>F<sub>8</sub> coolant leaks from the ATLAS silicon tracker into external N<sub>2</sub>-purged anti-humidity envelopes is better than 0.05 m s<sup>-1</sup>.

Taking the C<sub>4</sub>F<sub>10</sub>/N<sub>2</sub> combination example of Fig. 4, the C<sub>4</sub>F<sub>10</sub> concentration needed to match the refractivity of CF<sub>4</sub> is 16.3% (Table 1). At this concentration  $V_s$  is 233 ms<sup>-1</sup> and  $m$  is  $-0.22\%$  ms<sup>-1</sup>. A  $\delta V_s$  of 0.05 ms<sup>-1</sup> would result in  $\delta(w_i)$  of  $1.1 \times 10^{-4}$ .

### 3.3 From sound velocity to Cherenkov thresholds and GWP load

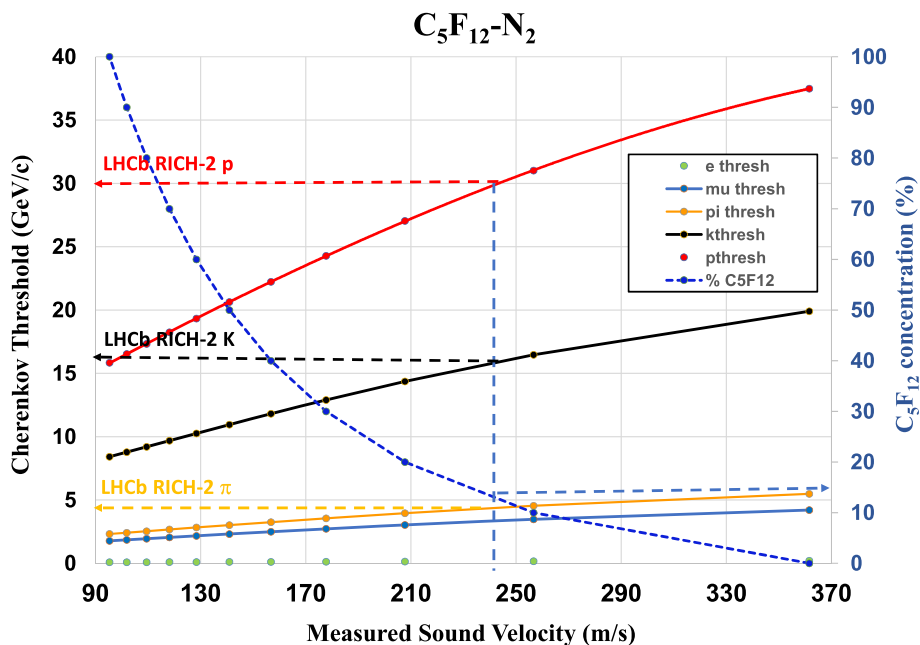
As illustrated in Fig. 4 the refractivity of the radiator gas can be found from the molar concentrations,  $w_i$ , and individual refractivities  $(n-I)_i$  of C<sub>4</sub>F<sub>10</sub> and N<sub>2</sub> via Eq. (2), leading to the  $\beta$  threshold and the thresholds in GeV for the different charged particle species. A measurement of sound velocity is a direct measurement of Cherenkov thresholds. The sound velocity range of Fig. 4 encompasses current transitions between passivation and active radiator in the COMPASS and LHCb RICH-1 detectors. Also shown on Fig. 4 (in brown, black and red on the left axis) are the  $\pi^\pm$ ,  $K^\pm$  &  $p^\pm$  thresholds for the LHCb RICH-2 CF<sub>4</sub> radiator.

The C<sub>4</sub>F<sub>10</sub> molar concentration in N<sub>2</sub> necessary to achieve these LHCb RICH-2 thresholds is around 16.3% (Table 1, line 7) at which the sound velocity is 233 ms<sup>-1</sup>. Such a C<sub>4</sub>F<sub>10</sub>/N<sub>2</sub> blend would reduce the radiator volume GWP load by 36% compared with a CF<sub>4</sub> radiator. A non-cyclic C<sub>4</sub>F<sub>8</sub>O molecule with similar optical and thermodynamic properties to C<sub>4</sub>F<sub>10</sub> would completely eliminate the GWP load of the second component.

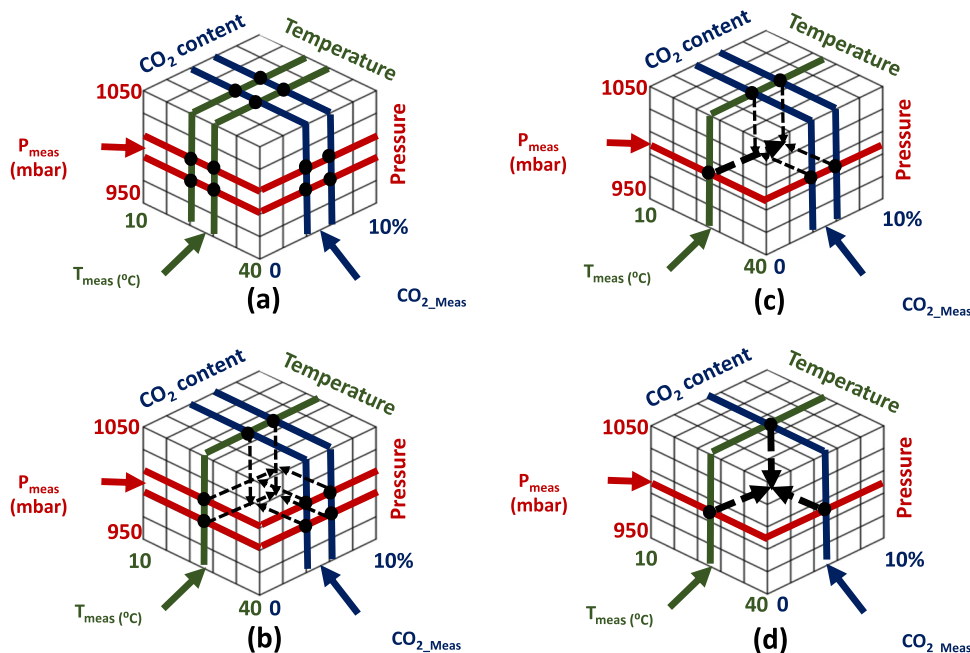
In the LHCb RICH-2 a few percent of CO<sub>2</sub> is currently added to the CF<sub>4</sub> radiator to suppress its scintillation light [29]. Figure 6 illustrates the variation in Cherenkov threshold with CO<sub>2</sub> concentration in CF<sub>4</sub>, starting from the assumption that CO<sub>2</sub> would be the radiator vessel protective passivation gas when the detector was not in operation. The current operating combination with a few percent of CO<sub>2</sub> gives a refractivity of around of  $483 \times 10^{-6}$  and  $\pi^\pm$ ,  $K^\pm$ ,  $p^\pm$  thresholds of 4.5, 16 and 30 GeV/c.

Figure 7 considers the corresponding case for C<sub>5</sub>F<sub>12</sub>/N<sub>2</sub> as a CF<sub>4</sub> substitute. The C<sub>5</sub>F<sub>12</sub> concentration to match the LHCb RICH-2  $\pi^\pm$ ,  $K^\pm$  &  $p^\pm$  thresholds is around 13% (Table 1, line 9) at which the sound velocity is around 235 ms<sup>-1</sup>. This blend reduces the radiator volume GWP load by 45% compared with a CF<sub>4</sub> radiator. Should NOVEC5110 (C<sub>5</sub>F<sub>10</sub>O) exhibit similar optical thermodynamic and material compatibility properties to C<sub>5</sub>F<sub>12</sub> its substitution—in a blend with nitrogen—for CF<sub>4</sub> (Table 1) would completely eliminate the GWP load.

**Fig. 7** Left: Cherenkov thresholds for particle species versus measured sound velocity in a radiator gas combining  $C_5F_{12}$  with  $N_2$ . Right:  $C_5F_{12}$  concentration. The  $C_5F_{12}$  concentration to match the LHCb RICH-2  $p^\pm$ ,  $K^\pm$  &  $\pi^\pm$  thresholds (with much lower GWP load: Table 1) is shown on the right axis



**Fig. 8** Schematic showing the three-step successive interpolation of sound velocity versus {FC in  $N_2$ } concentration fit parameters held in ‘cans’ (·) at the nearest stored grid intersections to determine those corresponding to the measured  $\{T, P, \%CO_2\}$  process conditions

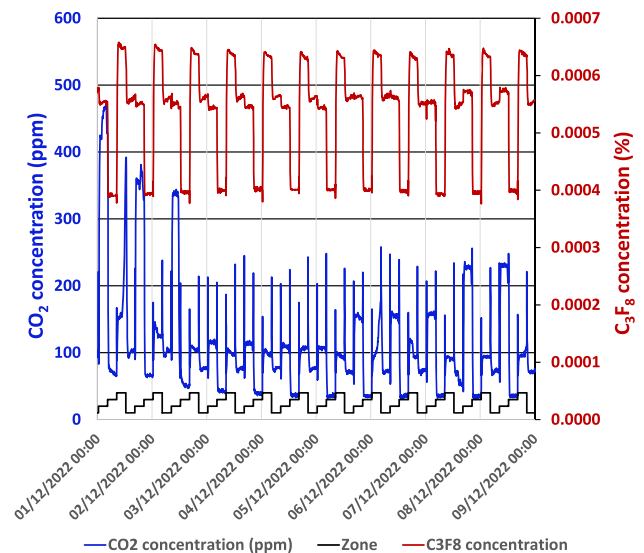


### 3.4 Database extension for background gases

LHCb RICH-2 currently operates with a mixture of  $CF_4$ ,  $N_2$ ,  $CO_2$  and  $O_2$  (from residual air) [30, 31]. Blends of “FCs” (fluorocarbons: either SFCs or NOVEC fluoro-ketone vapours) with  $N_2$  {FC in  $N_2$ } are well adapted to ultrasonic gas analysis due to their widely different component molecular weights. Such a blend can be analyzed by ultrasound in the presence of other background gases if their molar concentrations are also known through other instrumentation. Electrochemical cells can be used to monitor  $O_2$  concentration while non-dispersive Infra Red (NDIR) sensors can monitor  $CO_2$  levels. Thermodynamic data for all background gases, in the form of  $C_p$  and  $C_v$  over a grid of operating temperature and pressure must be available, however, so that sound velocity versus FC/ $N_2$  relative concentration can be calculated on a grid with known molar background gas compositions using Eqs. (4) & (5).

Figure 8 illustrates the case where a single background gas ( $CO_2$ ) is present in a FC/ $N_2$  radiator gas mixture. Since the sound velocity is measured at  $\{T_{meas}, P_{meas}, \%CO_{2meas}\}$  values that will not necessarily correspond exactly to stored  $\{T, P, \%CO_2\}$  grid points, interpolation is required.

**Fig. 9** Variations of % molar  $C_3F_8$  (red) and ppm  $CO_2$  conc. (blue) in 4 environmental zones of the ATLAS SCT silicon tracker. {Zones indicated by repeating staircase (black): (1) “barrel top” → (2) “barrel bottom” → (3) “end cap C” → (4) “end cap A” → (1)}



Fit parameters of  $\{FC \text{ in } N_2\}$  versus sound velocity generated using Eqs. (4) & (5) and stored in intersection ‘cans’ ( $\cdot$ ) on a 3-D  $\{T, P, \%CO_2\}$  grid are interpolated as shown in Fig. 8a–d. The 8 nearest grid points in  $(T, P, \%CO_2)$  space are chosen to define the smallest cuboidal volume encompassing the process measurables  $\{T_{\text{meas}}, P_{\text{meas}}, \%CO_{2,\text{meas}}\}$ . For clarity these eight points are represented as projections on the  $(P, T)$ ,  $(P, \%CO_2)$ , and  $(\%CO_2, T)$  facets in Fig. 8a.

The interpolation proceeds from the start position of Fig. 8a in three steps:

- The  $\{FC \text{ in } N_2\}$  versus sound velocity fit parameters held in the 8 “cans” depicted in Fig. 8a are interpolated to intermediate values corresponding to  $T_{\text{meas}}$  at grid pressures immediately above and below  $P_{\text{meas}}$  as shown in Fig. 8b, collapsing the search at the core of the grid to a 2-D search between four grid points on a square in  $\{P, \%CO_2\}$  space;
- These intermediate  $\{FC \text{ in } N_2\}$  versus sound velocity fit parameters are then interpolated along the orthogonal  $(P)$  direction to calculate new intermediate parameters corresponding to  $P_{\text{meas}}$  as shown in Fig. 8c, further collapsing the core search to a final interpolation between two adjacent grid points on a line in the  $\{\%CO_2\}$  direction;
- The final interpolation of intermediate  $\{FC \text{ in } N_2\}$  versus sound velocity fit parameters is then made along the  $\{\%CO_2\}$  direction to obtain the final parameters corresponding to  $\{P_{\text{meas}}, T_{\text{meas}}, CO_{2,\text{meas}}\}$ : Fig. 8d.

Figure 9 illustrates measurements of the concentrations of two gases of primary interest—here used in the context of fluorocarbon cooling of particle tracking detectors, a context further developed in §5.

Figure 9 illustrates (in red) the %  $C_3F_8$  coolant concentration leaking into the four  $N_2$ -purged environmental volumes of the ATLAS ‘SCT’ silicon tracker. The four zones, sampled in sequence in 4-h periods by aspiration through a single sonar instrument [23], have varying permeability (and hydrostatic collectivity) to  $CO_2$  ingress from the exterior; the sources being other ATLAS sub-systems employing  $CO_2$  in active gas mixtures for charged particle detection. Ingressed  $CO_2$  (illustrated in blue in Fig. 9) is monitored with a 10,000 ppm full-scale Amphenol Telaire<sup>®</sup> NDIR probe in series with the sonar tube. This instrument pairing allows unambiguous  $C_3F_8$  concentration measurement on top of a varying known  $CO_2$  concentration. During the measurement period of Fig. 9 the ingressed  $CO_2$  concentration underwent a decrease in one of the four SCT zones (1–3/12/2022) due to external manipulations of  $CO_2$  systems in other parts of ATLAS, while the  $C_3F_8$  concentration into each zone (from small  $C_3F_8$  coolant leaks in the SCT) remained stable.

In Fig. 9 the relative concentrations of a primary gas pair of interest ( $C_3F_8/N_2$ ) are demonstrably measured in four mixture streams—each containing different, variable, known concentrations of a third gas—the analysis using a data base including that gas, constructed using the formalism of eqs. (4) & (5) with the interpolation technique illustrated in Fig. 8.

In the case where a second background gas is present, the interpolation procedure acquires another step. Figures 10 and 11 illustrate the interpolation of  $\{FC \text{ in } N_2\}$  versus sound velocity for a gas pair of primary interest in the presence of four process variables: temperature, pressure,  $CO_2$ , and  $O_2$  (the gases, for example present in LHCb RICH-2) This is an interpolation of fit parameters calculated at the intersections of a four-dimensional grid which can be illustrated in a Coxeter B4 projection of the related tesseract.

It can be seen in Fig. 10 that opposite faces of the tesseract are formed by four pairs of cubes (colour-coded a–d) for identification). Three interpolations can be made within these cubes—in the same way as illustrated in Fig. 8—with the final interpolation made along the dimension that separates them. It is evident that the interpolation can be made in four different sequences, to arrive at the same result. These paths are illustrated by extraction and reduction in Fig. 11a–d.

**Fig. 10** Tesseract (Coxeter B4 projection) showing the four (color-coded) possible initial three-interpolation routes for  $\{FC_{in} N_2\}$  concentration versus sound velocity polynomial fit parameters within the 4-D  $\{P, CO_2, T, O_2\}$  database (a–d): respectively via the  $\{CO_2, O_2, T\}$ ,  $\{T, O_2, P\}$ ,  $\{CO_2, P, O_2\}$ , and  $\{CO_2, P, T\}$  pathways

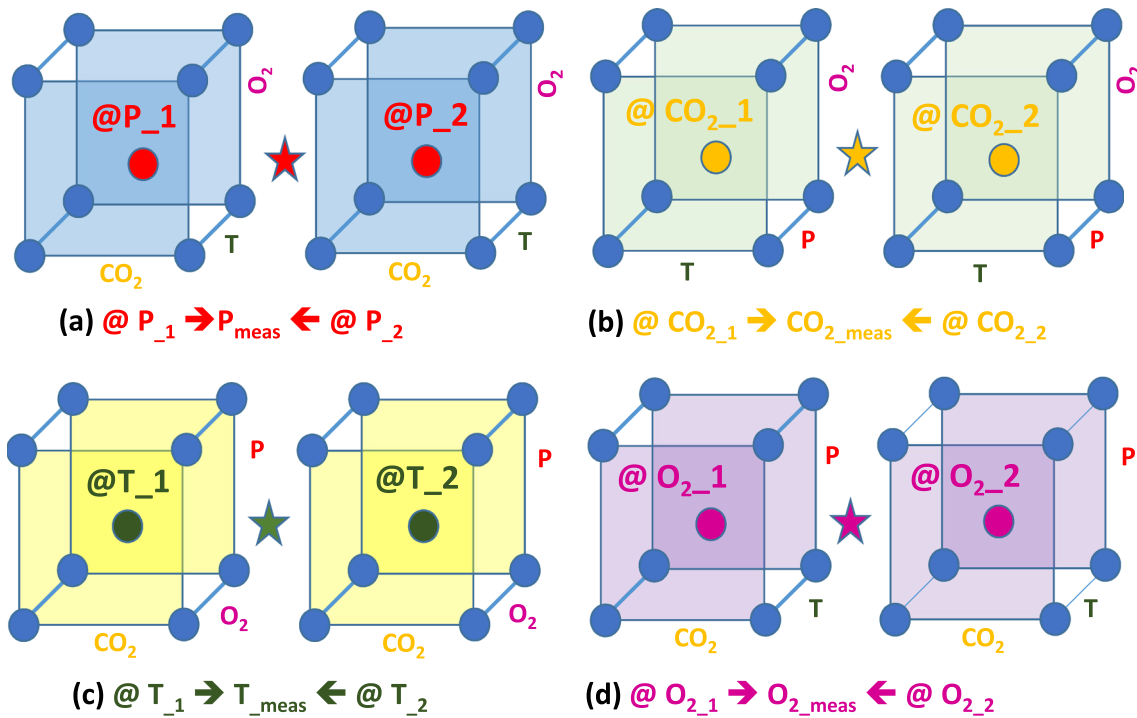
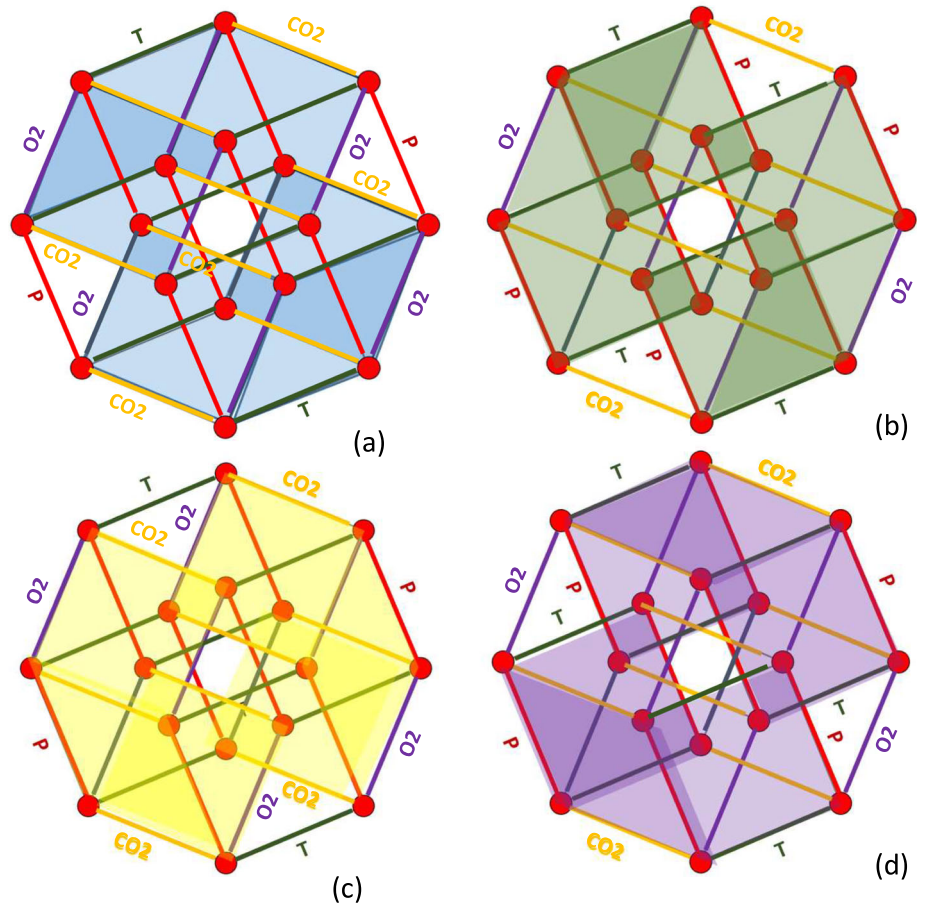
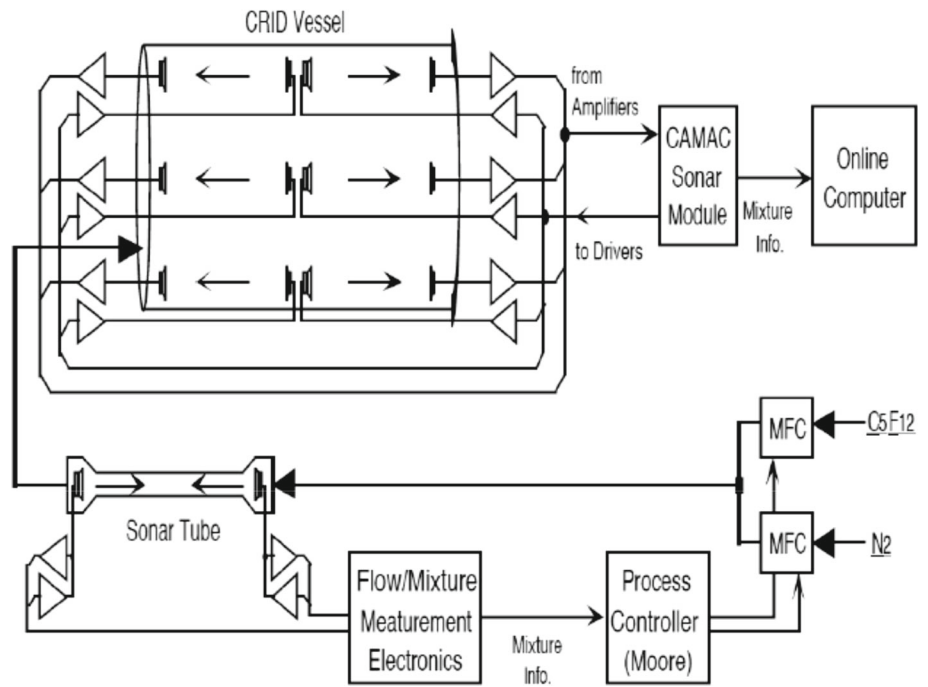


**Fig. 11** Final interpolation step between  $\{FC_{in} N_2\}$  concentration versus sound velocity polynomial fit parameters already interpolated to points within their respective cubes at opposite faces of the  $\{P, CO_2, T, O_2\}$  tesseract of Fig. 10

**Fig. 12** SLD barrel CRID multiple sonar installation for mixing C<sub>5</sub>F<sub>12</sub> and N<sub>2</sub> before injection into the gas radiator, and for measurement of refractive index in the radiator vessel [20–22]



Figures 10 and 11 illustrate the interpolations from regions of interest defined by the nearest grid points in dataspace. Multidimensional parameter interpolation (by sequential cube extraction) is less of a problem than the geometric growth in the number of data-points in the extradimensional databases.

With fine grid mesh fit parameter interpolations can be linear, but this leads to a large database, with a total number of parameters given by:

$$DBsize(\text{data points}) = \text{No. prim. fit coeffs.} \cdot \frac{RoI_T}{d_T} \cdot \frac{PRoI_P}{d_P} \cdot \frac{RoI_{Conc. \text{ bkd gas } 1}}{d_{Conc. \text{ bkd gas } 1}} \dots \tag{8}$$

where  $RoI_T, P, \text{ etc.}$  are the ranges of interest of the process variables and  $d_T, P, \text{ etc.}$  are their corresponding grid step sizes or granularities.

Database size may clearly be reduced by sparsifying the granularity in some dimensions (or eliminating them altogether by applying a physical law rather than a short-range interpolation). One example would be in the temperature dimension using the relation:

$$v_{s_{T_2}} = v_{s_{T_1}} \cdot \sqrt{\frac{T_2}{T_1}} \tag{9}$$

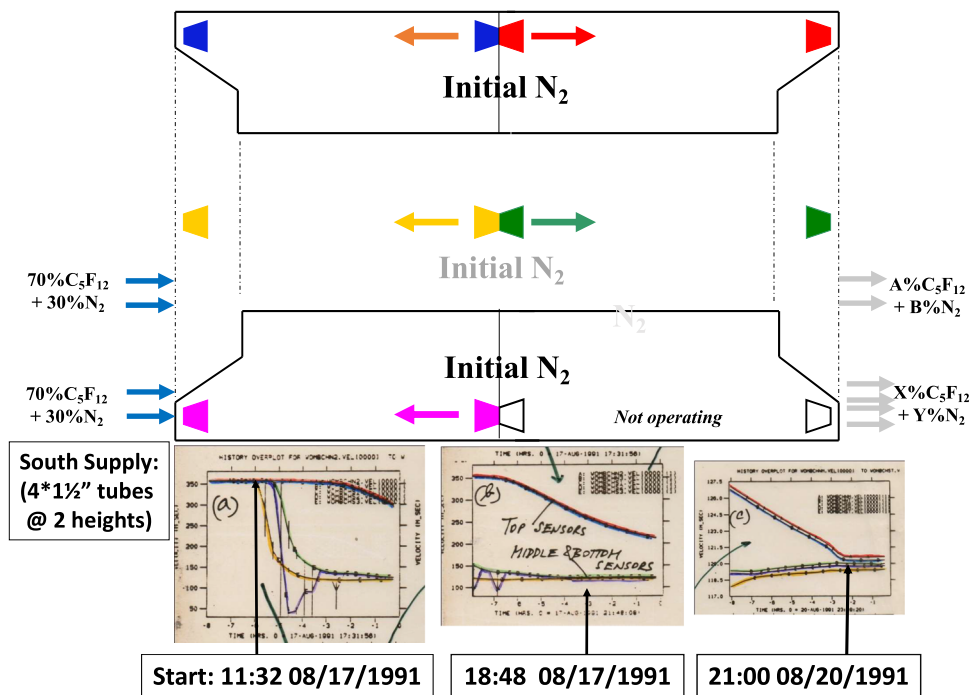
where  $v_{s_{T_1}}$  and  $v_{s_{T_2}}$  are the sound velocities at absolute temperatures  $T_1$  and  $T_2$  respectively. Alternatively, if the rate of change in sound velocity with another parameter (for example pressure) is low and predictable, the granularity in this dimension can be relaxed using fewer datapoints: the conceptual cubes of Figs. 8, 10 and 11 will in practice become elongated cuboids.

#### 4 Active control of radiator gas refractivity and uniformity

In the SLAC SLD barrel CRID application the radiator gas composition—and hence the refractive index—was monitored ultrasonically at multiple *in-situ* points at different heights in the 12 000 L radiator vessel using pairs of ultrasonic transducers positioned between the mirror array and the outer vessel wall at the 3, 6 and 12 o’clock azimuthal positions (Fig. 12). During the pre-commissioning of the detector in 1991 this system revealed significant hydrostatic stratification in the vessel when N<sub>2</sub> passivation gas was being replaced by a blended radiator. This effect is illustrated in Fig. 13, which shows the active sonar paths plots colour-coded to plots from the original commissioning logbooks [32].

Gas was initially (and simultaneously) injected into 12,000 L radiator vessel through four tubes at two locations within the bottom third of the vessel. Gas was initially recovered through 6 tubes, also within the bottom third of the vessel. During the gas transition phase a rapid decrease in sound velocity was seen in the sonars monitoring the mid (equatorial) zone and lower third of the vessel, with the sound velocity decreasing to within 10% of that expected in a C<sub>5</sub>F<sub>12</sub>/N<sub>2</sub> within around 7 h. The sound velocity in the upper third of the vessel however took 3½ days to drop to similar values, indicating inefficient sweeping of the radiator volume

**Fig. 13** Illustration of hydrostatic stratification seen in the multi-sonar installation during the early commissioning of the SLD barrel CRID, when  $N_2$  radiator passivation gas being replaced by a  $C_5F_{12}/N_2$  active mix [32]



compounded by possible flotation of light nitrogen passivation gas (m.w. 28) on top of the incoming blend containing  $C_5F_{12}$  (m.w. 288).

Based on these studies the gas supply and recovery ports were repositioned on the radiator vessel, with extra exit ports added in the upper third of vessel to boost the hydrostatic ejection rate of the nitrogen passivation gas during filling with the heavier active radiator gas.

It was clear from this study that careful placement of supply and exhaust ports were mandatory and that sufficient time was needed to allow gas homogenisation in a tall or crowded gas radiator volume—particularly with gases of very different molecular weight—before a uniform refractive index could be expected.

A blend of 87%  $C_5F_{12}$  /13%  $N_2$  was considered optimum for the required particle identification ranges. The blend was recirculated through a compressor-less thermosiphon in a continuous thermodynamic (condensation/evaporation) cycle. The  $C_5F_{12}$  vapour in the blend leaving the radiator vessel was condensed through heat exchange with cold  $N_2$  gas, evolving from the cooling loops of a liquid argon calorimeter, then stored in a cooled tank at  $-80\text{ }^\circ\text{C}$ —where its saturated vapour pressure was a few hPa—while the uncondensed  $N_2$  was allowed to escape. Liquid  $C_5F_{12}$  left the tank under gravity, entering an electrically-heated pot to be evaporated and added to a stream of fresh  $N_2$ . An ultrasonic gas analyzer monitored the circulating mixture in real-time and simultaneously acted as a flowmeter in a “pinched axial” geometry, sending sound signals in opposite directions in the flowing gas and using the transit time difference to calculate the flow rate.

When fully commissioned in 1996 with active feedback this sonar instrument also sent corrective signals to two mass flow controllers to dynamically tune 87%  $C_5F_{12}$  /13%  $N_2$  blend injected into the radiator vessel. Full active control of radiator gas blend and refractivity thereafter maintained the  $\beta = 1$  Cherenkov ring angle to long-term variation better than  $\pm 0.3\%$  [20] (Fig. 14).

The SLD CRID multi-sonar installation simplified detector commissioning by allowing a “data-independent” estimator of refractive index uniformity not totally reliant on measurement of the Cherenkov radius of  $\beta = 1$  particles, but confirmable through such measurements. It also remained in continuous 24/7 operation during data taking. This multi-sonar approach has been less-used in RICH detectors that have followed, but similar installations could be considered in the context of maintaining and circulating SFC or NOVEC blends with lighter carriers to reduce the overall GWP load of a Cherenkov gas radiator and to monitor uniformity of refractive index across the full height of the radiator volume.

## 5 Silicon tracking detector cooling with fluorocarbons, blends and fluoro-ketone NOVEC fluids

Fluorocarbons have been used in the electronics industry for more than 40 years. These uses include cooling, semiconductor manufacture and reflow vapour-phase soldering in the manufacture of large printed circuit boards. The Cray-2 supercomputer famously used 3 M FC77 Fluorinert<sup>®</sup> liquid for direct immersive cooling. The non-conductivity, non-flammability and radiation-

**Fig. 14**  $\beta = 1$  Cherenkov angle comparison (1995-6 runs) between reconstructed ring data ( $\square$ ) in the SLD barrel CRID and angles from sonar-deduced refractive index corrected for atmospheric pressure ( $\bullet$ ); [20] **a** without active sonar control of radiator blend, **b** with active control

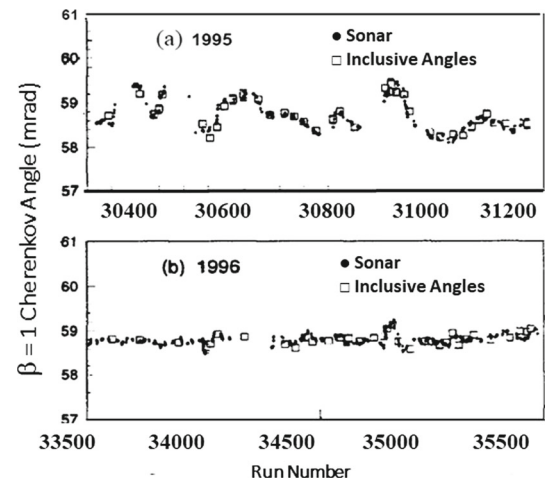


**Table 2** Main parameters of most currently-operating CERN-based silicon tracking detectors

Tracker	Tracker “DNA”*	Primary coolant: (liquid or evaporative)	Total cooling power (kW) and mass flow	On-detector tube coolant temp ( $^{\circ}\text{C}$ ) and pressure ( $\text{bar}_{\text{abs}}$ )	Typical Si module temp ( $^{\circ}\text{C}$ )
ATLAS (SCT $\mu$ -strips and pixels) [36]	Tube and block	$\text{C}_3\text{F}_8$ (E)	60 1.2 kg/s	SCT: $-26 \rightarrow -10$ $^{\circ}\text{C}$ 1.6 $\rightarrow$ 3 pixels: $-24.5$ $^{\circ}\text{C}$ 1.7	SCT: $-7 \rightarrow +7$ $^{\circ}\text{C}$ (layer, disk dependent) pixels: $-14.5$ $^{\circ}\text{C}$
ATLAS (IBL) [38]	Tube & block	$\text{CO}_2$ (E)	2 30 g/s	$-20$ $^{\circ}\text{C}$ 20	$-13$ $^{\circ}\text{C}$
CMS ( $\mu$ -strips) [33]	Tube & block	$\text{C}_6\text{F}_{14}$ (L)	34 (TIB, TID, TOB and TEC) 30 kg/s	$-15$ $^{\circ}\text{C}$ 6	$-10 \rightarrow 0$ $^{\circ}\text{C}$ (position dependent, single or double-sided modules etc.)
CMS Pixel [37]	Tube & block	$\text{CO}_2$ (E)	15 (max) 100 g/s	$-23$ $^{\circ}\text{C}$ 18	$-13$ $^{\circ}\text{C}$
LHCb VELO [39]	Micro-channel	$\text{CO}_2$ (E)	1.6 22.4 g/s	$-30$ $^{\circ}\text{C}$ 14	$-28$ $^{\circ}\text{C}$
TOTEM [35]	Tube & block	$\text{C}_3\text{F}_8$ (E)	1.2 40 g/s	$-26$ $^{\circ}\text{C}$ 1.6	$-15$ $^{\circ}\text{C}$
WA62 Gigatracker [34]	Micro-channel	$\text{C}_6\text{F}_{14}$ (L)	0.16 12 g/s	$-14 \rightarrow -12$ $^{\circ}\text{C}$ 3	5 $^{\circ}\text{C}$

\* See text

resistance of SFCs have made them ideal coolant choices for detectors in particle physics experiments:  $\text{C}_6\text{F}_{14}$  is used as a liquid coolant for electronics in many sub-detectors at LHC experiments.

### 5.1 Coolant examples from current silicon tracker cooling systems

The primary (on-detector) cooling systems of the silicon trackers of the LHC experiments are currently based mainly on SFCs. Liquid  $\text{C}_6\text{F}_{14}$  cools the CMS silicon microstrip tracker [33] and the NA62 Gigatracker [34], while evaporative  $\text{C}_3\text{F}_8$  cooling is used to cool silicon tracking detectors in the 24 Roman pots of the TOTEM detector [35] and the ATLAS SCT and pixel detectors [36]. The main cooling parameters of most currently-operating CERN-based silicon tracking detectors are shown in Table 2. Among these are the  $\text{CO}_2$  evaporative systems that cool the CMS pixel detector [37], the ATLAS IBL (“Insertable B Layer”) pixel detector [38] and the LHCb “VELO” (“VERTex LOCator”) [39].

These trackers are based on two main topologies (or types of “DNA”):

- “tube and block” geometry (in both barrel and end-cap disks), with silicon detector modules attached via cooling blocks to axially-, radially- or circumferentially-routed robust cooling tubes for trans-interface conductive heat removal. Coolant tubes may be in sliding grease contact with thermal supports onto which silicon detector substrates are glued (for example in the case of the ATLAS barrel pixel detector), may be embedded in heat conducting foam or may be rigidly attached to cooling blocks located under readout electronics at the periphery of silicon (microstrip) sensors;

**Table 3** Thermophysical Properties of NOVEC 649(C<sub>6</sub>F<sub>12</sub>O) and C<sub>6</sub>F<sub>14</sub> (at 25°C except where noted: after [40])

Fluid thermophysical property	NOVEC 649: C <sub>2</sub> F <sub>5</sub> C(O)CF(CF <sub>3</sub> ) <sub>2</sub> Perfluoro-2-methyl-3-pentanone (C <sub>6</sub> F <sub>12</sub> O fluoro-ketone)	C <sub>6</sub> F <sub>14</sub> (perfluorohexane, saturated fluorocarbon)
Boiling temp @ 1 atm (°C)	49	56
Critical temp (°C)	169	178
Critical pressure (MPa)	1.87	1.89
Freezing temperature (°C)	< - 100	< - 100
Specific heat (J kg <sup>-1</sup> K <sup>-1</sup> )	1103	1050
Density (kg m <sup>-3</sup> )	1610	1680
Kinematic viscosity (cSt)	0.42	0.4
Latent heat (J kg <sup>-1</sup> )	88	88
Vapour pressure @ 25 °C (kPa)	40.4	30.9
Vapour pressure @ 100 °C (kPa)	441	350
Water solubility (ppm <sub>w</sub> )	21	10

– micro-channel geometry: with micro-channel cooling channels (of cross section  $250 \times 150 \mu\text{m}$  or less) etched into heat-sinks for front-end readout electronics and the silicon detector modules themselves. This detector configuration is clearly more adapted to small systems, but has a thermal figure of merit (TFM) that can be superior by a factor of 10 or more compared to "tube and block" implementations. Expressed in units of  $^{\circ}\text{C cm}^2 \text{W}^{-1}$  as  $(T(\text{Si module}) - T(\text{Coolant})) / (\text{Si module power}/\text{cm}^2)$ , the lower the numeric TFM value the better the thermal performance. Microchannel-cooled devices can achieve TFM values of  $1.5\text{--}4 \text{ }^{\circ}\text{C cm}^2 \text{W}^{-1}$  [39] while tube-and-block implementations with longer heat paths and higher thermal impedances report TFM values between  $13 \text{ }^{\circ}\text{C cm}^2 \text{W}^{-1}$  [38] and  $25 \text{ }^{\circ}\text{C cm}^2 \text{W}^{-1}$  [41]

Liquid C<sub>6</sub>F<sub>14</sub> cooling is successfully used in the NA62 Gigatracker: the first silicon microchannel vertex detector [34]. Liquid cooling can be attractive in such detectors since such liquid circulation systems typically operate at lower pressures than (particularly) CO<sub>2</sub>-based evaporative cooling systems, although this latter technology has subsequently been mastered in the LHC VELO [39]. In its original version the LHCb VELO used evaporating CO<sub>2</sub> to cool microchannels in the substrates of front-end electronic tiles. In the recent upgrade for LHC run 2 [39] the original VELO detector has been replaced with a completely new detector incorporating CO<sub>2</sub>-based evaporative cooling in a system containing 52 directly-cooled heat sink modules, each substrate containing 14 ( $200 \times 70 \mu\text{m}$ ) micro-channeled cooling substrates to maintain a silicon pixel module operating temperature of  $-30 \text{ }^{\circ}\text{C}$ .

### 5.2 The substitution of perfluorohexane C<sub>6</sub>F<sub>14</sub> with C<sub>6</sub>F<sub>12</sub>O fluoro-ketone

Thermophysical properties of C<sub>6</sub>F<sub>14</sub> and NOVEC 649 (C<sub>6</sub>F<sub>12</sub>O) fluoro-ketone are listed in Table 3. Evident similarities have made the substitution of C<sub>6</sub>F<sub>14</sub> with NOVEC 649 a potentially attractive option in future liquid-cooled systems, and motivated a detailed comparative study [14] of NOVEC fluids with perfluorohexane C<sub>6</sub>F<sub>14</sub> (Fluotec<sup>®</sup> PPI: supplied by F2 Chemicals, Preston, UK).

The *as-received* purity of the NOVEC 649 samples for this study were in conformity with the CERN standard minimal purity requirement for C<sub>6</sub>F<sub>14</sub>. The radiation resistance (radiolytic destruction rate) of NOVEC 649 was determined at gamma doses up to 100 kGy and found to be comparable to that of C<sub>6</sub>F<sub>14</sub>. Due to the presence of oxygen, this fluoroketone is known to react with liquid water [40] to produce pentafluoropropionic acid (CF<sub>3</sub>CF<sub>2</sub>CO<sub>2</sub>H) which could be potentially corrosive to circulation systems. It is therefore necessary to keep moisture content at very low levels using standard desiccants. Molecular sieves and desiccants used traditionally in CERN C<sub>6</sub>F<sub>14</sub>-based systems proved efficient for use with C<sub>6</sub>F<sub>12</sub>O [14], with no indication of reactivity.

Following this study NOVEC 649 was proposed as a C<sub>6</sub>F<sub>14</sub> replacement for detector cooling applications at doses up to 100 kGy. Further investigations, including elastomer compatibility and the temperature dependence of hydrolysis effects, are ongoing at CERN, while data on common elastomers, including neoprene, butyl-, fluoro-, nitrile-, EPDM and silicone rubbers are also available from 3 M [40].

NOVEC 649 was chosen as the liquid coolant for the silicon photomultipliers (SiPMs) of the new LHCb scintillating fibre (SciFi) tracker [42] where the SiPMs must be kept at temperatures of  $-40 \text{ }^{\circ}\text{C}$  to reduce the dark count rate and retain single photon counting capability. To achieve this temperature cooling fluid must be circulated at  $-50 \text{ }^{\circ}\text{C}$  by the LHCb SciFi SiPM cooling system. This choice of a new, zero-GWP coolant for use at CERN was recently announced in an article for the general public [43].

### 5.3 The speculative substitution of saturated fluorocarbons with fluoro-ketones in evaporative cooling

Evaporative fluorocarbon cooling was pioneered [36] for use in the ATLAS pixel and SCT microstrip tracker. Octafluoropropane (C<sub>3</sub>F<sub>8</sub>) primary coolant was initially circulated using a compressor system, recently replaced (from 2018) by a gravity-driven thermosiphon [44] with a condenser located 90 m above the ATLAS detector. The compressor system now serves as a back-up



for the thermosiphon, which has the advantage of requiring no pumps or moving parts (with the exception of valves) in the  $C_3F_8$  primary coolant loop.

An additional study [45] using a full thermal- and fluidic- model of an on-detector ATLAS SCT cooling circuit [36] demonstrated that the "drop-in" substitution of  $C_3F_8$  with a 75% $C_3F_8$ /25% $C_2F_6$  molar zeotropic blend could reduce the operating temperature of the ATLAS SCT silicon microstrip tracker by 9 °C with no change to the external cooling circuitry. While the use of blends can extend the operational life of an existing detector to larger accumulated radiation doses than originally anticipated, the extra complexity of mixing is not recommended for new installations, where as far as possible a pure fluid should be matched to the temperature cycle.

Concern has been raised that  $CO_2$  cooling may be unable to maintain silicon tracker modules at low enough operating temperatures for adequate protection against leakage current-induced thermal runaway over the full High Luminosity program of LHC; currently scheduled to run from 2029 to late 2041 [46]. This limitation is related to the relatively high  $CO_2$  triple point temperature of  $-56$  °C and the known loss in  $CO_2$  system performance below  $-40$  °C [47]. The maintenance of adequate safety margins (operating temperatures sufficiently below the expected onset temperatures of thermal runaway) becomes more critical as silicon modules accumulate high radiation doses during the HL-LHC profile. These concerns have led to the exploration of alternative approaches, including the use of krypton evaporative cooling in a transcritical thermodynamic cycle and even blends of  $CO_2$  with nitrous oxide ( $N_2O$ ) [48].

Such safety margins will be dependent on detector fabrication technology and distance from the LHC interaction points. It can be surmised, however, by extrapolation from the silicon *module-coolant* temperature offsets of Table 2 in current (pre-HL) LHC operation that the lower thermal figure-of-merit of trackers built in the "tube and block" geometry will require lower coolant evaporation temperatures than microchannel devices, particularly should the thermal conductivity of the heat evacuation path degrade with material exposure to high radiation doses. For example, higher silicon *module-coolant* temperature offsets in the range 15–20 °C are expected in certain regions of the upgraded ATLAS ITk silicon tracker being built for operation at HL-LHC [41].

A practical constraint in an evaporative cooling system is that the vapour pressure of coolant leaving the on-detector evaporative cooling channels should exceed around 1.5 bar<sub>abs</sub>. This represents a conservative safety factor of 500 mbar above the minimum desirable compressor aspiration pressure and allows for the pressure drop in external piping returning vapour to compressors. A thermosiphon or compressorless system would ideally operate under similar conditions; for example in a passive thermosiphon a minimum pressure of at least 1 bar<sub>abs</sub> would be desirable at the bottom of the vertical tube returning vapour against gravity to the colder condenser.

Figure 15 compares pressure-enthalpy ( $p-h$ ) diagrams for (a) octafluoropropane ( $C_3F_8$ ), (b)  $CO_2$ , (c) hexafluoroethane ( $C_2F_6$ ) and (d) xenon (Xe). Full circulator thermodynamic cycles are not drawn, as these are highly system-dependent—for example with reversed rotation directions in the case of compressor [36] versus thermosiphon [44] or pumped accumulator [49] operation—and beyond the scope of this work. Nonetheless, some conclusions can be drawn from the bare  $p-h$  diagrams using simple indices.

On each  $p-h$  diagram red indices illustrate the fluid vapour pressure at an ambient temperature around 20 °C, from which detectors must be cooled to their operating temperatures. These pressures are, respectively, around 7.6, 57, 30 and 58 bar for  $C_3F_8$ ,  $CO_2$ ,  $C_2F_6$ <sup>2</sup> and Xe.<sup>3</sup> It can be seen that  $CO_2$  or xenon cooled systems will require the highest pressure tolerance by a large factor. This is further amplified since typical test and compliance pressures are typically more than a factor of two higher than the highest expected operation pressure [39].

In the case of  $C_3F_8$  (Fig. 15a)—currently used in the ATLAS and TOTEM detectors—it is clear that the combination of an *in-tube* evaporation temperature of  $-50$  °C at a minimal exhaust pressure of 1.5 bar<sub>abs</sub> is thermodynamically impossible, clearly excluding this fluid for many future installations. However the dual constraints can be met with in  $CO_2$ ,  $C_2F_6$  and Xe (blue indices in Fig. 15b, c and d) with respective exhaust pressures of 6.8, 4 and 12 bars. In the case of  $CO_2$  however  $-50$  °C is very close to the triple point temperature of  $-56$  °C and probably represents the minimum safe system temperature. Of the four fluids  $C_2F_6$  and xenon offer the best promise from a thermodynamic perspective, but  $C_2F_6$  has a very high global warming potential and is likely to be prohibited in the near future.

Xenon is clearly a thermodynamic alternative to  $C_2F_6$ , as shown in Fig. 15d. It is a non-flammable radiation-resistant noble gas with a molecular weight (131) very close to that of  $C_2F_6$  (138). There is considerable experience in its purification and thermodynamic circulation in dark matter detectors, where it is used in large (multi-tonne) quantities. This fluid is unlikely however—due to its scarcity and extremely high cost—to find use in secondary applications such as tracking detector cooling.

It is likely that all SFC fluids will be eliminated from use at CERN in the next decade. However following the  $C_6F_{14}/C_6F_{12}O$  NOVEC649 and  $C_5F_{12}/C_3F_{10}O$  NOVEC 5110 analogy it is probable that new zero-GWP NOVEC-like fluids with spurred oxygen-bearing molecules of the form  $C_2F_4O$  (m.w.116) and  $C_3F_6O$  (m.w.166) would have similar thermodynamic and thermophysical properties to their similar molecular weight SFC analogues -  $C_2F_6$  (m.w.138) and  $C_3F_8$  (m.w.188). Although the industrialisation of new such fluids will probably depend on future demand from the electronics industry as replacements for SFCs, as has been the case for previously-developed zero-GWP NOVEC fluids, enquiries and approaches to industry should certainly be contemplated.

<sup>2</sup> The critical temperature and pressure of  $C_2F_6$  are 19.8 °C & 30.4 bar<sub>abs</sub>.

<sup>3</sup> The critical temperature and pressure of Xe are 16.6 °C & 58.4 bar<sub>abs</sub>.

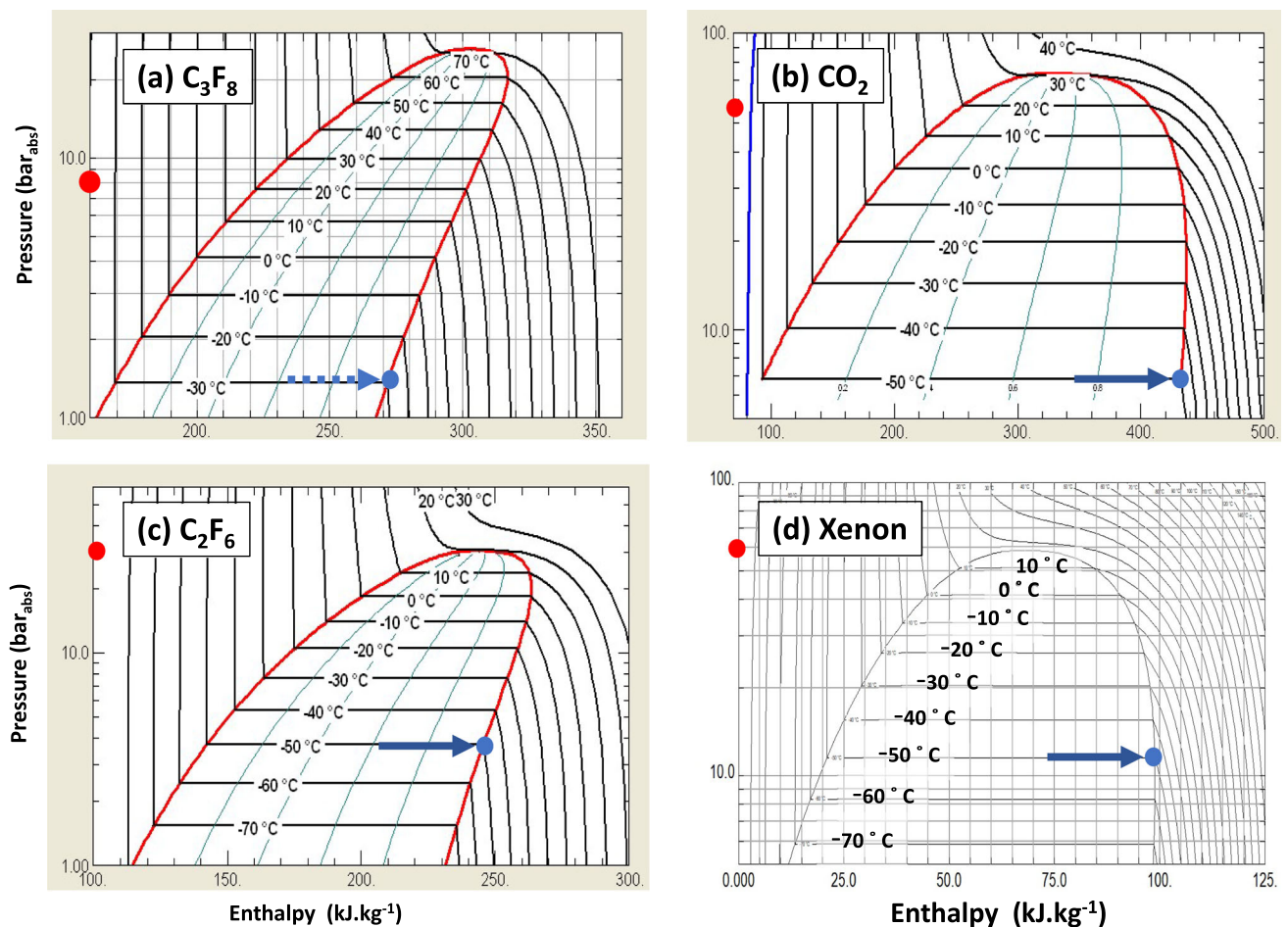


**Fig. 15** Pressure-enthalpy ( $p-h$ ) diagrams for **a**  $C_3F_8$ , **b**  $CO_2$ , **c**  $C_2F_6$  and **d** Xe. Red indices: saturation pressure at which cooldown from ambient temperature starts. Blue indices: (a)  $C_3F_8$  minimum practical in-tube evaporation temperature for a pressure of 1.5 bar<sub>abs</sub>; (b), (c) and (d) evaporation pressures in  $CO_2$ ,  $C_2F_6$  and Xe for the example of an in-tube evaporation temperature of  $-50^\circ C$ ; see text

#### 5.4 Ultrasonic Leak detection

Continuous and stringent leak monitoring is necessary, as in the case of Cherenkov radiators. In ATLAS a sonar system [50] (Fig. 16) was developed to monitor gas extracted from the nitrogen-flushed environmental anti-humidity volumes of the silicon pixel and IBL detectors and from four points in the three separate environmental volumes of the SCT silicon microstrip tracker, generating operator alarms when the concentration of coolant exceeded predefined thresholds.

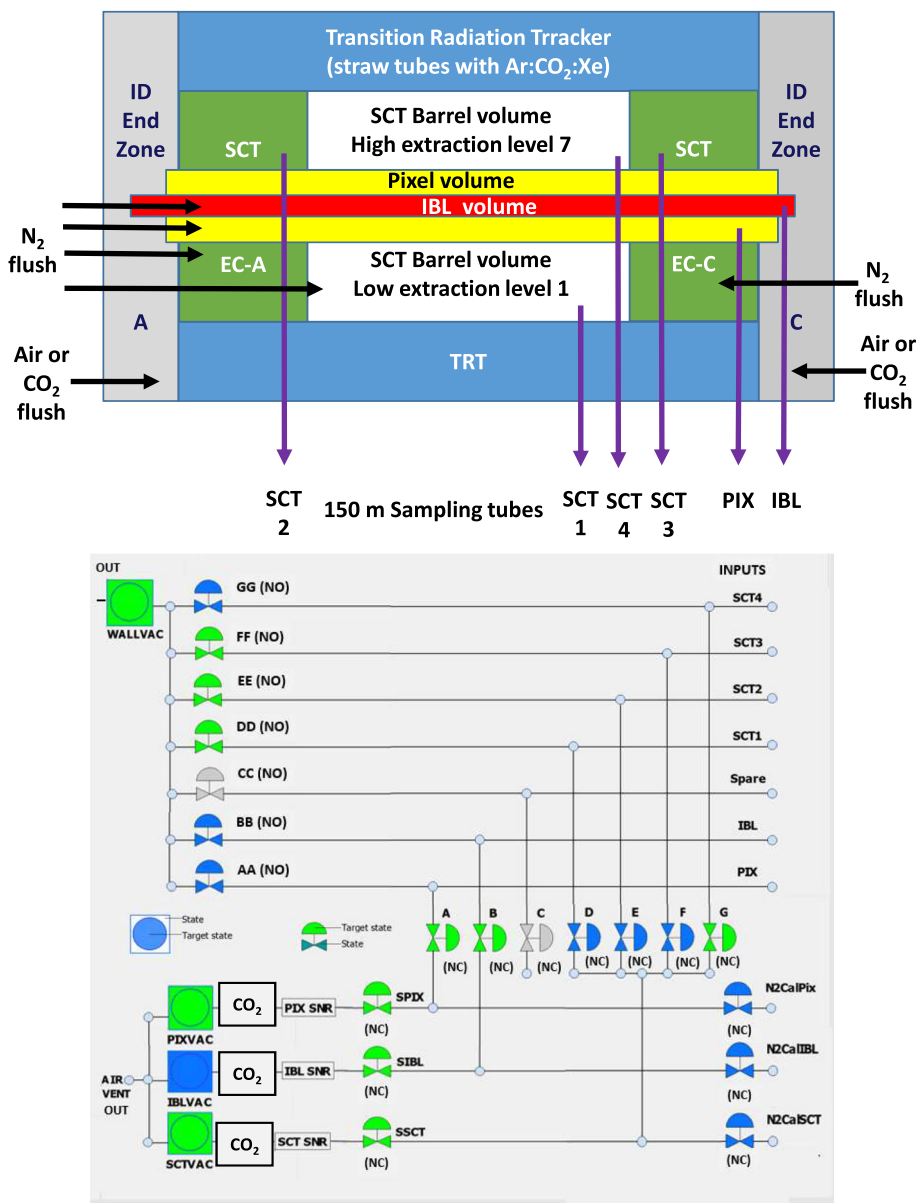
Gas is aspirated using membrane pumps<sup>4</sup> at typical flow rates of 4 L/min through six 150 m sampling tubes from the ATLAS inner detector. Aspirated gas passes through three 50 cm sonar tubes equipped with pairs of Senscomp<sup>®</sup> model 600 ultrasonic transducers [28] and three Amphenol Telaire<sup>®</sup> 10,000 ppm full scale NDIR  $CO_2$  monitors.

All instruments, pumps and valves are interfaced to the ATLAS detector control system using custom electronics, with gas stream sampling controlled via remotely-operated normally-open (NO) and normally-closed (NC) pneumatic valves, which also allow periodic sonar recalibration with nitrogen reference gas. SCT zones 1–4 are monitored in sequence via NC valves **D–G**. The three tubes from the unmonitored SCT zones at any particular time are aspirated by a fourth pump via NO valves **DD–GG**, reducing the sonar reaction time by preventing gas stagnation within the 150 m sampling tubes.

An example and discussion of results from the SCT sonar was given in Fig. 9 in the context of the multi-gas analysis algorithm depicted graphically in Fig. 8 (§ 3.4). This system operates permanently 24/7 with a sensitivity to  $C_3F_8$  (m.w. 188) ingress into  $N_2$  (m.w. 28) of  $10^{-5}$ . Even better sensitivity can be expected in a future system for the detection of trace leaks of heavy molecular weight fluids such as  $C_6F_{12}O$  (m.w. 316)  $C_5F_{10}O$  (m.w. 266) into  $N_2$  (or dry air) atmospheres: one candidate application might be the leak detection of NOVEC 649 ( $C_6F_{12}O$ ) which has been chosen for SiPM cooling in the LHCb detector [42, 43]. It is clear that retention volumes equipped with selective and sensitive alarm-generating leak detection systems will be necessary wherever

<sup>4</sup> KNF Neuberger model N811KNE; max. vol. flow 11.5 l/min @ 1 bar<sub>abs</sub>.

**Fig. 16** The coolant leak monitoring system of the ATLAS silicon tracker. Upper: gas sampling points in the nitrogen-purged environment volumes of the IBL, pixel and SCT sub-detectors. Lower: view of the arrangement of aspiration pumps, remote control selection valves and sonar tubes (Siemens symatic graphical user interface). SCT1-4 are sequentially sampled by SCTSNR in four-hour periods via remote control NC valves *D–G*



saturated fluorocarbons or fluoro-ketone fluids are used, due to the expense of the cooling fluids. The installation of such systems should be a priority in any strategy to reduce fluorinated fluid escape, wastage and environmental contamination.

**6 Conclusion**

This paper has considered the general use of saturated fluorocarbons (SFCs:  $C_nF_{(2n+2)}$ ) and non-cyclic spur-oxygenated  $C_nF_{2n}O$  “GWPzero” fluoro-ketone fluids in the context of Cherenkov radiator media and detector cooling for high radiation environments. The paper has further explored the blending of high-order saturated fluorocarbon (SFC) or fluoro-ketone vapours with a light carrier gas to replicate the refractive index of  $CF_4$  and  $C_4F_{10}$  with the aim of reducing or eliminating the GWP “load” (tonnes  $CO_2$  equivalent) of large volume Cherenkov gas radiators. Should the currently-available NOVEC5110 fluoro-ketone ( $C_5F_{10}O$ ) exhibit similar optical and thermodynamic properties to  $C_5F_{12}$  its *in-blend* substitution for  $C_4F_{10}$  and  $CF_4$  would completely eliminate the GWP loads of the COMPASS and LHCb RICH detectors.

NOVEC 5110,  $CF_2O$ , and non-cyclic forms of  $C_4F_8O$  could be chosen for particular attention (approaches to industrial manufacturers followed by measurements of optical and thermodynamic properties) for use as future blendants in RICH gas radiators.

Although these fluids do not yet exist in large quantities over the full  $C_nF_{2n}$  “matrix” the radiation tolerance and thermal performance of NOVEC 649 ( $C_6F_{12}O$ ) is sufficiently promising for it be chosen by LHCb as a  $C_6F_{14}$  replacement for the cooling

silicon photomultipliers of the new scintillating fibre tracker. Since the NA62 Gigatracker [34] successfully used  $C_6F_{14}$  liquid cooling, NOVEC649 may also turn out to be a good substitute for the liquid cooling of future silicon microchannel vertex detectors built in technologies (and/or with inter-module connectivity) unable to resist the high maximum test pressures (160 bars) typical of  $CO_2$  evaporative cooling systems. Such vertex detector cooling systems would contain a relatively small volume of liquid coolant.

A new  $C_2F_4O$ -structured evaporative coolant could be a thermodynamic substitute for  $C_2F_6$  or xenon to achieve silicon temperatures of  $-40\text{ }^\circ\text{C}$  or lower in “block and tube” tracker configurations operated at high luminosity below the practical temperature limit for  $CO_2$  evaporative cooling systems.

Nonetheless, it is clear that pressure will continue to reduce the use of fluorinated materials. On Feb 7th 2023 the European Chemical Agency (ECHA) published a proposed list of more than 10 000 per- and polyfluoroalkyl (PFA) materials of high concern to be investigated for future use or restriction [51–54]. It is intended that ECHA’s scientific committees will evaluate the proposal in terms of the risks to people and the environment, and impact on society. The eventual outcome of this process might be the cessation of fabrication of most of the range of the SFC (particularly) and NOVEC-like products, along with the development of new fluoro-ketone species.

Since the use of large-volume flammable or high-pressure gas Cherenkov radiators would be extremely problematic in CERN’s underground spaces an alternative solution might involve the blending of low molar concentrations of heritage-stock higher-order SFCs with transparent lighter gases at atmospheric pressure. For example,  $C_4F_{10}$  from stock for the COMPASS and LHCb RICH-1 radiators could be blended at low molar concentration with nitrogen or argon to replicate the refractive index of  $CF_4$  in the LHCb RICH-2 radiator with a lower overall GWP load. This reductive substitution might be seen as an advantageous “deferred destruction” use of existing SFC stock.

Ultrasonic binary gas mixture analysis techniques-initially used for Cherenkov radiator refractometry at the SLAC SLD CRID have been recently refined with new algorithms to allow analysis of a gas pair of primary interest in the presence of background gases. These techniques are well adapted to this new challenge, and for the detection of leaks of such high molecular weight vapours into lighter gases including air. Such installations should be more widely used to monitor leaks, in conjunction with secondary containment volumes added where possible, wherever SFCs or NOVEC fluids are used in Cherenkov radiators and cooling applications.

**Acknowledgements** I would like to thank Helen McNamee and Andy Penman of F2 Chemicals, Preston, UK, also Christophe Frei and Antonello di Mauro of CERN for valuable discussions on the current availability of fluorocarbons for use as Cherenkov gas radiators. Jaroslav Vavra of SLAC is thanked for his recollections of the SLD CRID commissioning. I also thank Paola Tropea and Erik Butz of CERN and Nick Lumb of Centre de Physique des Particules de Marseille (CPPM) for sharing thermal operation details of the CMS silicon tracker; also Martin Doubek (CERN), Koichi Nagai (Oxford University) and Alexandre Rozanov (CPPM) for similar data on the TOTEM and the ATLAS IBL, SCT and pixel detectors. Thanks also go to Eric Vigeolas (CPPM) and Joleen Pater (Manchester University) for information on the expected thermal performance of elements of the upgraded ATLAS ITK silicon tracker under HL-LHC conditions. I thank Paula Collins and Wiktor Byczynski (CERN) for extensive information on the LHCb VELO and Mathieu Perrin-Terrin (CPPM) for information on the NA62 Gigatracker. I also thank Sune Jacobsen (CERN) for information concerning the cooling of the LHCb Scintillating fibre tracker. Their help is much appreciated: any eventual misinterpretations are solely due to the author.

**Data availability** Data sharing not applicable to this article as no datasets were generated or analysed during the current study.

## Declarations

**Conflict of interest** The author has no relevant financial, non-financial or competing interests to declare that are relevant to the content of this article. The author has no financial or proprietary interests in any material discussed in this article.

**Open Access** This article is licensed under a Creative Commons Attribution 4.0 International License, which permits use, sharing, adaptation, distribution and reproduction in any medium or format, as long as you give appropriate credit to the original author(s) and the source, provide a link to the Creative Commons licence, and indicate if changes were made. The images or other third party material in this article are included in the article’s Creative Commons licence, unless indicated otherwise in a credit line to the material. If material is not included in the article’s Creative Commons licence and your intended use is not permitted by statutory regulation or exceeds the permitted use, you will need to obtain permission directly from the copyright holder. To view a copy of this licence, visit <http://creativecommons.org/licenses/by/4.0/>.

## References

1. CERN Environment Report 2017–2018 <https://doi.org/10.25325/CERN-Environment-2020-001>
2. B. Mandelli, Eco-gas mixtures and mitigation procedures for Green-house Gases (GHGs); ECFA Detector R&D Road-map Symposium: T.F. 1 Gaseous Detectors, (2021) [https://indico.cern.ch/event/999799/contributions/4204191/attachments/2236047/3789965/BMandelli\\_ECFA.pdf](https://indico.cern.ch/event/999799/contributions/4204191/attachments/2236047/3789965/BMandelli_ECFA.pdf)
3. B. Mandelli, R&D for the optimization of the use of greenhouse gases in particle detector systems; Mini workshop on gas transport parameters for present and future generation of experiments: CERN (2021) <https://indico.cern.ch/event/1022051/contributions/4325947/>
4. G. Rigoletti, Studies to reduce greenhouse gas emissions from detectors at the LHC, (2022) EP-DT Seminar May 4, 2022.pdf (cern.ch)
5. S. Dalla Torre et al, Long term experience with  $C_4F_{10}$  in COMPASS RICH-1; Presentation 11th Intl. Workshop on Ring Imaging Cherenkov detectors, Edinburgh, Scotland, (2022). [https://indico.cern.ch/event/1094055/contributions/4932286/attachments/2508724/4311387/RICH2022\\_C4F10\\_dallatorre.pdf](https://indico.cern.ch/event/1094055/contributions/4932286/attachments/2508724/4311387/RICH2022_C4F10_dallatorre.pdf)

6. 3M PFG-3480: c-octofluorotetrahydrofuran (C<sub>4</sub>F<sub>8</sub>O). Note: fluid out of production: product reference now used for a non-fluidic product. For historic product data sheet mentioning its high GWP see (for example): (2023) [http://static6.arrow.com/aropdfconversion/a7116f41dfdd5b79d2eb7b40afd687f8af23d8ef/mediawebsserver\(563\).pdf](http://static6.arrow.com/aropdfconversion/a7116f41dfdd5b79d2eb7b40afd687f8af23d8ef/mediawebsserver(563).pdf)
7. M. Artuso et al., Nucl. Instr. Meth. A **558**, 373–387 (2006)
8. Product #2H07-2-08 Synonyms: 2,2,3,3,4,4,5,5-octafluorotetrahydrofuran, Perfluorotetrahydrofuran; CAS No: 773-14-8, MDL No. MFCD00465561: SynQuest Labs Inc., 13201 Rachael Boulevard, Alachua, FL 32615, USA <https://www.synquestlabs.com/Home/ProductDetail?SearchText=Octafluorotetrahydrofuran>
9. T. Acconcia et al., Nucl. Instr. & Meth. A **767**, 50–60 (2014)
10. M. Vollmer et al., Abundances, emissions, and loss processes of the long-lived and potent greenhouse gas octafluorooxolane (octafluorotetrahydrofuran, c-C<sub>4</sub>F<sub>8</sub>O) in the atmosphere. Atmos. Chem. Phys. **19**, 3481–3492 (2019)
11. 3M Novec® range of fluorinated fluids; [https://www.3m.com/3M/en\\_US/p/c/b/novec/?Ntt=novec](https://www.3m.com/3M/en_US/p/c/b/novec/?Ntt=novec)
12. 3M Novec 649/1230 fluid (C<sub>6</sub>F<sub>12</sub>O); <https://multimedia.3m.com/mws/media/5698650/3m-novec-engineered-fluid-649.pdf>, <https://multimedia.3m.com/mws/media/1246880/3m-novec-1230-fire-protection-fluid.pdf>
13. 3M Novec 5110 fluid (C<sub>5</sub>F<sub>10</sub>O); <https://multimedia.3m.com/mws/media/11321230/3m-novec-5110-insulating-gas.pdf>
14. CERN report EN-CV 22/12/2017, EDMS 1751219 2017-334 rev 1.0: Technical note NOVEC fluids qualification report: report on the study executed for the qualification of the NOVEC Fluid for detector cooling applications
15. J. Owens, Understanding the stability and environmental characteristics of a sustainable Halon alternative. 3M Performance Materials 3M Center, St. Paul, MN 55144 (2003)
16. CERN Mini-workshop on gas transport parameters for present and future generation of experiments 20/04/2021; S. Easo; LHCb-RICH detectors and their gas radiators <https://indico.cern.ch/event/1022051/contributions/4333562/attachments/2231064/3780374/LHCb-RICH-Current-GasRadiators-April-2021.pdf>, Options for alternate radiators in LHCb-RICH system (including calculations by O. Ullaland); S. Easo, <https://indico.cern.ch/event/1022051/contributions/4319538/attachments/2231436/3781060/LHCb-RICH-Future-Radiators.pdf>
17. S. Easo, Nucl. Inst. & Meth. A **876**, 168–173 (2017)
18. E. Lemmon, M. Huber, M. McLinden, REFPROP standard reference database 23, version 9.0 (2010) U.S. National Institute of Standards & Technology
19. E. Nappi, J. Seguinot, Rivista del Nuovo Cimento **28**, 8–9 (2005). <https://doi.org/10.1393/ncr/i2006-10004-6>
20. K. Abe et al., IEEE Trans. Nucl. Sci. **45**, 648–7705 (1998). <https://doi.org/10.1109/23.6826>
21. G. Hallewell et al., Nucl. Instr. Meth. A **264**, 219–234 (1988)
22. G. Hallewell, Nucl. Instr. Meth. A **876**, 50–53 (2017)
23. G. Hallewell et al., MDPI Instr. **5**(1), 6 (2021)
24. P. Stassi et al, Ultrasonic Gas mixture analysis system in the Forward RICH of DELPHI, DELPHI Internal Note 95-124 RICH73 (1995)
25. M. Sannino, Nucl. Instr. and Methods Phys. Res. A. **595**, 208–211 (2008)
26. C. D’Ambrosio et al, Monitoring, alignment and control of the RICH detectors; LHCb-Memo-2000-80 RICH (2000)
27. P. Fauland, PhD thesis; (COMPASS experiment) University of Bielefeld (2004)
28. Now marketed as SensComp model 600 transducer, <http://www.senscomp.com/ultrasonic-sensors/>
29. T. Blake et al., Nucl. Instr. Meth. A **791**, 27–31 (2015)
30. A. Papanestis, Nucl. Instr. Meth. A **766**, 14–18 (2014)
31. R. Calabrese et al., JINST **17**, P07013 (2022)
32. J. Vavra (SLAC National Laboratory); private communication
33. P. Tropea, The CMS tracker fluorocarbon cooling system, Engineering Forum: experiences from cooling systems for LHC detectors (2008) P. Tropea, E. Butz (CERN); private communications
34. G. Aglieri Rinella et al, JINST 14 P07010 M. Perrin-Terrin (CPPM); private communication (2019)
35. G. Anelli et al, JINST 3 S08007 M. Doubek (CERN); private communication (2008)
36. D. Attree et al, JINST 3 P07003 K. Nagai (Oxford), A. Rozanov (CPPM), private communications (2008)
37. W. Adam et al, JINST16P02027 CMS Technical Design Report for the Pixel Detector Upgrade CMS-TDR-011, CERN-LHCC-2012-016 07/09/2012, (2021)
38. ATLAS Insertable B-Layer Technical Design Report; CERN-LHCC-2010–013 ATLAS TDR 19 15/09/2010 A. Rozanov (CPPM); private communication
39. O. de Aguiar Francisco et al, Nucl. Instr. Meth. A. 1039, 166874 (2022) <https://www.sciencedirect.com/science/article/pii/S0168900222003394>. P. Collins & W. Byczynski (CERN); private communications
40. P. Tuma Fluoroketone C<sub>2</sub>F<sub>5</sub>C(O)CF(CF<sub>3</sub>)<sub>2</sub> as a Heat Transfer Fluid for Passive and Pumped 2-Phase Applications; 3M Co., 3M Center, 236-2B-01St. Paul, MN 55144, USA, Proc. 2008 IEEE 24th IEEE Semiconductor Thermal Measurement and Management Symposium, San Jose CA, (2008) <https://doi.org/10.1109/STHERM.2008.4509386>. Also accessible via: [https://twiki.cern.ch/twiki/pub/LHCb/SciFiDemoCooling/F.Tuma\\_c6K\\_as.....pdf](https://twiki.cern.ch/twiki/pub/LHCb/SciFiDemoCooling/F.Tuma_c6K_as.....pdf)
41. D. Alvarez et al, Thermo-Mechanical Performance of the Local Supports for the ATLAS ITk Pixel Outer Barrel: Experimental and FEA Studies; Forum on Tracking Detector Mechanics Tuebingen Germany. E. Vigeolas (CPPM), J. Pater (Manchester University); private communications (2023)
42. L. Gruber et al., Nucl. Instr. Meth. **958**, 162025 (2020)
43. C. Frei, S. Gambetta, B. Leverington, Building the future of LHCb, CERN Courier, September 2021 (2021) <https://cerncourier.com/a/building-the-future-of-lhcb>
44. M. Battistin et al., Int. J. Chemical Reactor Engineering. **13**(4), 511–521 (2015)
45. R. Bates et al., JINST **10**, P03027 (2015)
46. <https://lhccommissioning.web.cern.ch/schedule/LHC-long-term.htm>
47. L. Contiero et al, Cold krypton system for the phase III upgrade of the LHC, Forum on tracking detector mechanics, Tuebingen Germany May (2023)
48. L. Contiero et al, Krypton, applied as refrigerant for cooling of silicon detector trackers; GL 2022: 15th IIR-Gustav Lorentzen conference on natural refrigerants, Trondheim, Norway, (2023)
49. B. Verlaat, CO<sub>2</sub> cooling experiences in the LHCb velo thermal control system engineering forum: experiences from cooling systems for LHC detectors (2008)
50. R. Bates et al., JINST **8**, P02006 (2013)
51. ECHA/NR/23/04, <https://echa.europa.eu/-/echa-publishes-pfas-restriction-proposal>
52. ECHA Candidate List of substances of very high concern for Authorisation; <https://echa.europa.eu/candidate-list-table>
53. Annex to the Annex XV restriction report proposal for restriction: Per- & polyfluoroalkyl substances (PFASs); ECHA; 22/03/2023 <https://echa.europa.eu/documents/10162/d27fce1-b089-c4fd-1101-2601f53a07d1>
54. Per- and polyfluoroalkyl substances (PFAS); ECHA <https://echa.europa.eu/hot-topics/perfluoroalkyl-chemicals-pfas>